FBXO7/ntc and USP30 antagonistically set the basal ubiquitination threshold for mitophagy

Alvaro Sanchez-Martinez[1]*, Aitor Martinez[1], Alexander J. Whitworth[1]*

[1]MRC Mitochondrial Biology Unit, University of Cambridge, Cambridge Biomedical Campus, Hills Road, Cambridge, CB2 0XY, United Kingdom.

*Correspondence should be addressed to A.S.M. (e-mail alvaro.sanchez@mrc-mbu.cam.ac.uk) or A.J.W. (e-mail a.whitworth@mrc-mbu.cam.ac.uk)

Short title: FBXO7/ntc regulates basal mitophagy *in vivo*

Key words: FBXO7, ntc, PINK1, Parkin, USP30, pS65-Ub, mitophagy, Parkinson's Disease

Abstract

Functional analyses of genes linked to heritable forms of Parkinson's disease have revealed fundamental insights into the biological processes underpinning pathogenic mechanisms. Mutations in *PARK15/FBXO7* cause autosomal recessive PD and FBXO7 has been shown to regulate mitochondrial homeostasis. We investigated the extent to which FBXO7 and its orthologue in *Drosophila* ntc share functional homology and explored its role in mitophagy *in vivo*. We show that *ntc* mutants partially phenocopy *Pink1* and *parkin* mutants and *ntc* overexpression supresses *parkin* phenotypes. Furthermore, ntc can modulate mitophagy in a Pink1- and parkin-independent manner by promoting the ubiquitination of OMM proteins, a mechanism that is opposed by the deubiquitinase USP30. This basal ubiquitination serves as the substrate for Pink1-mediated phosphorylation which triggers damage-induced mitophagy. We propose that FBXO7/ntc works in equilibrium with USP30 to provide a checkpoint for mitochondrial quality control in basal conditions *in vivo* and presents a new avenue for therapeutic approaches.

Introduction

Parkinson's disease (PD) is the second most common neurodegenerative disorder. Autosomal recessive mutations in the genes encoding the mitochondrial kinase PINK1 (*PINK1*) and the E3 ubiquitin ligase Parkin (*PRKN*) are associated with parkinsonism. These genes have been shown to function in a common mitochondrial quality control pathway whereby mitochondria are degraded by autophagy (mitophagy). Briefly, PINK1 is partially imported to healthy polarised mitochondria where it is cleaved and subsequently degraded in the cytosol (Yamano and Youle, 2013). Upon mitochondrial depolarisation, PINK1 is stabilised on the outer mitochondrial membrane (OMM) where it phosphorylates ubiquitin-Ser65 (pS65-Ub) coupled to OMM proteins (Okatsu et al., 2015a; Okatsu et al., 2015b). This acts as signal for Parkin to be recruited and phosphorylated, relieving its autoinhibitory conformation, and allowing it to further ubiquitinate proteins in close proximity (Gladkova et al., 2018; Sauve et al., 2018) that will serve as additional substrates for PINK1 creating a feed-forward mechanism (Ordureau et al., 2014). Counteracting mitochondrial ubiquitination, USP30, a mitochondrial outer membrane deubiquitinase, removes Ub from Parkin substrates acting as a negative regulator of mitophagy (Bingol and Sheng, 2016). The accumulation of pS65-Ub on the OMM triggers the recruitment of autophagy receptors, which promote autophagosome recruitment and, ultimately, degradation of the damaged mitochondria (Lazarou et al., 2015; Yamano et al., 2020).

However, most of our understanding of the function of PINK1 and Parkin come from the utilisation of mitochondrial uncouplers or inhibitors in cultured cells, usually in conjunction with Parkin overexpression (Lazarou et al., 2015; Pickrell and Youle, 2015). Hence, there is a need to understand these mechanisms in more physiological model systems. *Drosophila melanogaster* models have delivered fundamental insights into the physiological function of the homologues *Pink1* and *parkin* (adopting FlyBase nomenclature), providing an excellent system to study mitochondrial homeostasis (Clark et al., 2006; Greene et al., 2003; Park et al., 2006; Poole et al., 2008; Whitworth et al., 2005; Ziviani et al., 2010). Interestingly, while proteomic analysis of mitochondrial turnover in *Drosophila* supports a role of Pink1/parkin in mitochondrial quality control (Vincow et al., 2013), studies using a pH-sensitive fluorescent mitophagy reporter showed that Pink1 and parkin had minimal impact on basal mitophagy (Cornelissen et al., 2018; Kim et al., 2019; Lee et al., 2018; McWilliams et al., 2018). Thus, many questions endure regarding the mechanisms of action Pink1/parkin in mitochondrial quality control *in vivo* and the potential contribution of other key players.

Mutations in the gene encoding F-box protein 7 (*FBXO7)*, have been found to cause autosomal recessive early-onset parkinsonism similar to those caused by mutations in *PINK1* and *PRKN* (Di Fonzo et al., 2009; Zhou et al., 2018), motivating a need to understand how FBXO7 is related to PINK1/Parkin biology. F-box domain-containing proteins are essential factors of the SCF-type (Skp1-Cul1-F-box) E3-ubiquitin ligase complexes, which are responsible for recruiting ubiquitin target substrates via the F-box domain (Skowyra et al., 1997). FBXO7 has both SCF-dependent and SCF-independent activities (Hsu et al., 2004; Kirk et al., 2008). Although it has been previously shown to cooperate with PINK1 and Parkin in mitophagy, (Burchell et al., 2013), how this occurs *in vivo* is poorly characterised warranting further investigation in an animal model. *Drosophila* encode a single homologue of *FBXO7* called *nutcracker* (*ntc*), which was identified in a screen for genes that control caspase activation during a late stage of spermatogenesis (Bader et al., 2010). ntc shares sequence, structure, and some functional similarities with mammalian FBXO7 (Bader et al., 2010; Bader et al., 2011; Kirk et al., 2008) and has been shown to regulate proteasome function via its binding partner PI31, an interaction that is conserved in FBXO7 (Bader et al., 2010; Bader et al., 2011). Thus, *Drosophila* provides a genetically tractable system to study role of ntc/FBXO7 in mitochondrial quality control *in vivo*.

Mitochondrial quality control mechanisms are believed to have an important pathophysiological role in PD. However, how this process is orchestrated *in vivo* and the upstream factors involved are still unclear. Therefore, we sought to investigate the relationship between ntc, Pink1 and parkin, and their role in basal mitophagy. We have found that ntc is able to compensate for the absence of *parkin* but not *Pink1*. Moreover, ntc plays an important role in promoting basal mitophagy in a Pink1- and parkin-independent manner, which is opposed by its counteracting partner USP30. This mechanism sets a threshold for basal mitophagy by regulating the steady-state levels of ubiquitin on OMM proteins, subsequently modulating the levels of pS65-Ub. Together, we provide evidence of a novel checkpoint for basal mitophagy that could potentially serve as therapeutic target for neurodegenerative disorders.

Results

Overexpression of *ntc* can rescue parkin but not Pink1 mutant phenotypes

The F-box domain localised in the C-terminal of *Drosophila* ntc shares considerable sequence similarity with that of human FBXO7 (Bader et al., 2010). Both proteins have a conserved valine residue involved in substrate recognition, including the common interacting partners, e.g. PI31 (Bader et al., 2011; Kirk et al., 2008). However, a functional conservation in between FBXO7 and ntc has not been formally tested *in vivo.* Notably, it has been shown that FBXO7 functionally interacts with mammalian PINK1 and Parkin and genetically interacts with *parkin* in *Drosophila* (Burchell et al., 2013). Therefore, as an initial exploration of the functional homology between ntc and FBXO7, we tested for a similar genetic interaction between *ntc* and *parkin. Drosophila parkin* mutants present multiple disease-relevant phenotypes, including locomotor deficits, dopaminergic neurodegeneration, and a severe mitochondrial disruption leading to flight muscle degeneration (Greene et al., 2003; Whitworth et al., 2005). Strikingly, overexpression of *ntc* by the strong ubiquitous *daughterless* (*da*)-GAL4 driver significantly rescued these *parkin* phenotypes, (Fig. 1A-D). At the molecular level, we observed that ntc is also able to decrease the steady state levels of the *Drosophila* Mitofusin (MFN1/MFN2) homologue Marf, which has been previously shown to be increased in *parkin* mutants (Ziviani et al., 2010) (Fig. 1E). These results support a functional homology between FBXO7 and ntc, and, moreover, indicate that ntc can at least partially substitute for parkin *in vivo*.

In contrast, assessing the functional relationship between ntc and Pink1 in a similar manner, ntc overexpression was unable to rescue climbing or flight locomotor defects of *Pink1* mutants, nor the increased Marf steady state levels (Fig. 1F-H). Furthermore, the neurodegenerative 'rough eye' phenotype induced by *Pink1* overexpression – commonly used for testing genetic interactors (Song et al., 2013; Whitworth et al., 2008) – was not enhanced by *ntc* overexpression as previously shown for *parkin* (Poole et al., 2008). These results mirror equivalent analyses of *FBXO7* (Burchell et al., 2013), and indicate that *Pink1* and *ntc* do not obviously genetically interact.

***ntc* mutants partially phenocopy *Pink1/parkin* mutants**

If ntc performs similar functions to the Pink1/parkin pathway in *Drosophila*, we reasoned that *ntc* mutants may phenocopy *Pink1/parkin* mutants. Supporting this, *ntc* mutants, like *Pink1* and *parkin* mutants, are male sterile due to defective sperm individualization (Bader et al., 2010; Clark et al., 2006; Greene et al., 2003; Park et al., 2006; Riparbelli and Callaini, 2007). To extend this, we assessed *ntc* mutants for classic *Pink1/parkin* phenotypes as described above. *ntc* mutants homozygous for an amorphic nonsense mutation (ntc^{ms771}; abbreviated as $ntc^{-/-}$) showed a marked defect in climbing and flight ability (Fig. 2A, B). We verified this using a hemizygous condition ($ntc^{-/Df}$) with comparable results (Fig. 2A, B). Importantly, transgenic re-expression of *ntc* was able to significantly rescue the climbing and flight deficit (Fig. 2A, B), confirming that the phenotype is specifically caused by loss of ntc function. Also similar to *Pink1/parkin* mutants, *ntc* mutants showed a dramatically shortened lifespan, with median survival of ~7 days compared to ~55 days for controls (Fig. 2C), which was almost completely rescued by transgenic re-expression of *ntc* (Fig. 2C).

However, in contrast to *Pink1/parkin* mutants, we did not observed loss of DA neurons in the PPL1 clusters of *ntc* mutants, although the short lifespan limited the analysis to only 10 days old (Fig. 2D). Likewise, immunohistochemical analyses of *ntc* mutants revealed no apparent disruption of mitochondrial morphology or integrity at confocal or electron-microscopy levels in flight muscle (Fig. 2E) or larval central nervous system (CNS) (Fig. 2F). Analysing mitochondrial respiratory capacity, *ntc* mutants were not consistently different from controls despite a downward trend (Fig. 2G). Nevertheless, ATP levels were reduced in *ntc* mutants (Fig. 2H), which was rescued by re-expression of wild-type *ntc*.

Oxidative stress is a consistent feature of PD pathology and normal ageing. Many models of PD show sensitivity to oxidative stressors such as paraquat (PQ), including *Drosophila parkin* mutants (Malik et al., 2015; Meulener et al., 2005). Similarly, *ntc* mutants also showed increased sensitivity to PQ exposure (Fig. 2I). Together, these results show that loss of *ntc* causes previously undescribed phenotypes that impact organismal vitality similar to *Pink1/parkin* mutants, though the effects are generally less severe.

ntc regulates basal mitophagy and antagonises USP30 in a Pink1 and parkin independent manner

Previous work showed that FBXO7 facilitates PINK1/Parkin-mediated mitophagy upon mitochondrial depolarisation in cultured cells (Burchell et al., 2013). Thus, we next sought to determine whether *Drosophila* ntc acts to promote mitophagy *in vivo*. The *mito*-QC reporter provides a sensitive and robust reporter for mitophagy whereby the GFP of OMM-localised tandem mCherry-GFP is quenched in the acidic lysosome, revealing mitolysosomes as 'mCherry-only' puncta (Allen et al., 2013). Importantly, in the absence of potent mitochondrial toxins – not readily applicable *in vivo* – the steady-state analysis of *mito*-QC provides an insight into basal mitophagy (Lee et al., 2018; Shen et al., 2021). Quantifying mitophagy in larval neurons revealed a significant reduction in *ntc* mutants compared to controls, which was rescued upon re-expression of *ntc* (Fig. 3A, B). Conversely, *ntc* overexpression significantly increased mitophagy (Fig. 3C, D). To verify these results, we analysed an alternative mitophagy reporter with a mitochondrial matrix-targeted version of *mito-QC*, termed MQC^{matrix}, with equivalent results (fig. S1A, B). Thus, ntc is both necessary and sufficient to promote basal mitophagy. Similarly, transgenic expression of *FBXO7* also increased mitophagy in larval neurons, underscoring their shared functionality (fig. S2A, B). Further validating these results in human cells stably expressing the *mito*-QC reporter (Montava-Garriga et al., 2020), siRNA-mediated knockdown of *FBXO7* also significantly reduced basal mitophagy (fig. S2C-E). Together these results support a conserved function of FBXO7/ntc in regulating basal mitophagy.

While 'stress-induced' mitophagy has been extensively studied, especially in cells, mechanisms regulating basal mitophagy are poorly characterised *in vivo*. Under basal conditions loss of *USP30*, an established regulator of basal mitophagy, leads to accumulation of ubiquitinated OMM proteins, and sustained *USP30* loss or inhibition promotes mitophagy *in vitro* (Bingol et al., 2014; Marcassa et al., 2018; Ordureau et al., 2020; Phu et al., 2020; Rusilowicz-Jones et al., 2020), but *in vivo* characterisation

remains limited. Upon *USP30* knockdown we observed a significant increase in basal mitophagy in larval neurons, using the both *mito*-QC (Fig. 3E, F) and MQC^{matrix} reporters (fig. S1A, B), and in adult flight muscle (fig. S3A, B). These results indicate that USP30 indeed inhibits basal mitophagy *in vivo* as expected. Importantly, we found that the induction of basal mitophagy by loss of *USP30* requires the activity of ntc as it was abolished in a *ntc* mutant background (Fig. 3E, F).

As an orthogonal approach to test for genetic interaction at the organismal level, we found that *USP30* overexpression caused a locomotor defect. This phenotype was completely suppressed by co-expression of *ntc* (Fig. 3G), consistent with the opposing actions of Ub-ligase and deubiquitinase and supporting the idea of ntc acting upstream of USP30. Interestingly, while *parkin* overexpression also suppressed the *USP30* overexpression phenotype as expected (fig. S3C), other Ub-ligases linked to mitophagy, Mul1 and March5 (Chen et al., 2017; Koyano et al., 2019; Ordureau et al., 2020; Rojansky et al., 2016; Yun et al., 2014; Zheng et al., 2022), showed no suppression of this phenotype (fig. S3C). Moreover, similar to *parkin* loss (Lee et al., 2018) or overexpression (fig. S3D, E), loss of Mul1 or March5 had no effect on basal mitophagy (fig. S3F-I). Together, these data highlight the specificity of ntc and USP30 as important and opposing regulators of basal mitophagy.

Given the previously established links between FBXO7 and USP30 with toxin-induced PINK1/Parkin mitophagy in cultured human cells, we next analysed whether the induction of basal mitophagy by *ntc* overexpression or *USP30* knockdown involved the *Pink1/parkin* pathway. As previously reported (Lee et al., 2018), the absence of *parkin* or *Pink1* did not impact basal mitophagy in larval neurons (Fig 4A-D). However, overexpression of *ntc* was still able to induce mitophagy in the absence of either *parkin* or *Pink1* (Fig. 4A-D). Likewise, *USP30* knockdown also increased mitophagy independently of *parkin* and *Pink1* (Fig. 5A-D), consistent with *in vitro* findings (Liang et al., 2015; Marcassa et al., 2018; Ordureau et al., 2020; Pan et al., 2021). Notably, the induction of mitophagy by *USP30* knockdown in *Pink1* or *parkin* mutant backgrounds required the function of *ntc* (Fig 5A-D), further underscoring the importance of ntc in basal mitophagy.

General autophagy is not grossly affected upon USP30 or ntc manipulations
Although previously validated as a reliable mitophagy reporter *in vivo*, we nevertheless verified that the increased mitolysosome formation (mitophagy) by *ntc* overexpression or *USP30* knockdown occurs via canonical autophagy flux as it was abrogated in the

absence of *Atg8a*, the main fly homologue of human ATG8 family members GABARAP/LC3, in both wild-type or *parkin* mutant backgrounds (fig. S4A-D). Notwithstanding, the observed increase in mitolysosomes could be due to an increase in non-selective autophagy (Lazarou et al., 2007; Nguyen et al., 2016). Thus, we used a number of well-established orthogonal assays to assess the effect of these mitophagy-inducing manipulations on general autophagy.

First, we examined the level of lipidated Atg8a (Atg8a-II) which is conjugated onto autophagosomal membranes and is used as an indication of autophagy induction (Jipa et al., 2021; Yoshii and Mizushima, 2017). Neither *USP30* knockdown, *ntc* overexpression nor *ntc* loss had any effect on autophagy induction (Fig. 6A, B). Similarly, the steady-state levels of ref(2)P, the homologue of mammalian p62, which accumulates upon autophagic blockage (Lorincz et al., 2017), were also not affected in any of the conditions (Fig. 6C, D). We also analysed the autophagy flux reporter GFP-mCherry-Atg8a (Low et al., 2013; Mauvezin et al., 2014; Nagy et al., 2014). Quantification of mCherry-Atg8a puncta (autolysosomes) showed no changes upon manipulating levels of *USP30* or *ntc* (Fig. 6E, F). Together, these results support that the effect observed upon manipulation of *USP30* or *ntc* is specific in basal mitophagy and not a consequence of altered general autophagy flux.

ntc increases basal mitochondrial ubiquitin and promotes phospho-ubiquitin formation

To gain a mechanistic insight into the regulation of basal mitophagy by ntc and USP30, we analysed their impact on mitochondrial ubiquitination. Consistent with their molecular functions, both *ntc* overexpression and *USP30* knockdown increased the total amount of ubiquitin present on isolated mitochondria under basal conditions (Fig. 7A, B). Indeed, recent studies indicate that USP30 acts to remove pre-existing OMM ubiquitin under basal conditions, possibly controlling the threshold needed for Parkin activation (Gersch et al., 2017; Marcassa et al., 2018).

We have recently described that loss of *parkin* causes a significant accumulation of pS65-Ub, consistent with parkin promoting the degradation of pS65-Ub labelled mitochondria (Usher et al., 2021). Unlike loss of *parkin*, loss of *ntc* alone did not have an effect on pS65-Ub (Fig. 7C, D). However, loss of *ntc* in a *parkin* mutant background (i.e., *parkin*:*ntc* double mutants) caused a significant reduction of pS65-Ub levels that would otherwise accumulate in *parkin* mutants (Fig. 7C, D). Furthermore, overexpression of *ntc* in the *parkin* mutant background resulted in an increase of pS65-

Ub compared to *parkin* mutant alone (Fig. 7E, F). These results are consistent with ntc promoting basal mitochondrial ubiquitination, which is acted upon by Pink1 to drive mitophagy. Thus, together these data suggest that ntc and USP30 work antagonistically to set up an OMM ubiquitin threshold needed for subsequence mitochondrial clearance.

Discussion

Mutations in *FBXO7* have been linked to familial parkinsonism but the mechanisms of pathogenesis are poorly understood (Di Fonzo et al., 2009; Zhou et al., 2018). We have characterized the putative *Drosophila* homologue, *ntc*, to assess the functional homology with *FBXO7* and its potential as a model to understand the function of FBXO7 *in vivo*.

FBXO7 has been genetically linked to *Drosophila Pink1* and *parkin* and shown to facilitate PINK1/Parkin-mediated mitophagy *in vitro*. Over the past two decades, the *Drosophila* models have provided valuable insights into Pink1/parkin biology, particularly in mitochondrial homeostasis, and been used to establish a number of key genetic interactors. Here we show that *ntc* mutants partially phenocopy *Pink1/parkin* phenotypes in locomotor function, lifespan and sensitivity to paraquat, consistent with a role in mitochondria quality control. We also observed the same genetic relationship as previously reported for *FBXO7* (Burchell et al., 2013); namely, that overexpression of *ntc* can rescue all *parkin* mutant phenotypes but not for *Pink1* mutants. These findings support a functional homology between ntc and FBXO7.

Importantly, FBXO7 has previously been shown to facilitate the PINK1/Parkin pathway to promote ‘damage-induced’ mitophagy *in vitro* (Burchell et al., 2013; Zhou et al., 2015). However, whether it regulates mitophagy *in vivo* is poorly characterised. Indeed, mitophagy itself can occur via different regulators and stimuli, and represents only one of several mechanisms of mitochondrial quality control (Ashrafi and Schwarz, 2013; Pickles et al., 2018). For instance, most studies have utilised a mitochondrial toxification stimulus to model substantial ‘damage’, however, basal mitophagy occurs as a housekeeping-type mechanism to regulate quantity or piecemeal turnover. The development of genetically encoded mitophagy reporters has provided a powerful approach to monitor both damage-induced or basal mitophagy *in vivo*. We have shown here that ntc is able to modulate basal mitophagy in a Pink1- and parkin-independent manner, which is conserved by FBXO7 in human cell lines.

In comparison to damage-induced mitophagy, the regulation of basal mitophagy is poorly characterised, particularly in metazoa. While early studies showed the mitochondrial deubiquitinase USP30 antagonises PINK1/Parkin-mediated mitophagy (Bingol et al., 2014; Cunningham et al., 2015; Ordureau et al., 2015), recent studies have established a role in basal mitophagy (Marcassa et al., 2018; Ordureau et al., 2020; Phu et al., 2020; Rusilowicz-Jones et al., 2020). The emerging view suggests the main role of USP30 is acting as part of a quality control process for intra-mitochondrial proteins during import through the translocon (Ordureau et al., 2020; Phu et al., 2020), and that basal mitochondrial ubiquitination provides the initiating substrate for PINK1 signalling. This paradigm requires a Ub ligase to provide basal ubiquitination that USP30 acts upon. While Phu et al. (Phu et al., 2020) suggested that this may be mediated via March5, this was not concurred by Ordureau et al. (Ordureau et al., 2020). Thus, the ligase providing the basal ubiquitination is unclear, and the role of USP30 in basal mitophagy *in vivo* remained to be established.

Here we demonstrated that knockdown of USP30 *in vivo* does indeed increase basal mitophagy in neurons and muscle, consistent with the *in vitro* studies. This also established a paradigm with which to more deeply analyse the function of ntc in basal mitophagy. While the induction of basal mitophagy by *USP30* knockdown is Pink1/parkin independent as expected, it nevertheless required the function of ntc. In contrast, overexpression of parkin or depletion of either Mul1 or March5 did not affect neuronal basal mitophagy in our assay. The antagonistic relationship between USP30 and parkin was also evident from genetic interactions at the organismal level (rescue of a climbing defect), as expected, and was recapitulated with ntc. Such an interaction was also not evident with Mul1 and March5. Mechanistically, we found that *ntc* promotes mitochondrial ubiquitination under basal conditions, which was mirrored by the downregulation of USP30, consistent with the idea that basal ubiquitination signals basal mitophagy. Thus, our data suggest that ntc/FBXO7 provides basal ubiquitination, that is antagonised by USP30, which facilitates basal mitophagy upon a yet unclear stimulus.

The current mechanistic view of PINK1/Parkin signalling posits that upon mitochondrial depolarisation or import clogging PINK1 becomes stabilised in the translocon, phosphorylates latent or pre-existing Ub, which promotes recruitment of Parkin, triggering the feed-forward mechanism. Ubiquitination of import substrates would provide a ready source of latent Ub for PINK1 to phosphorylate as/when it becomes

activated. Interestingly, USP30 has been found to be associated with TOMM20, a bona fide substrate of FBXO7 (Teixeira et al., 2016), and other translocon assemblies, where basally ubiquitinated translocon import substrates accumulate (Ordureau et al., 2020). Consistent with ntc providing the basal ubiquitination in this model, pS65-Ub that accumulates in *parkin* mutants is both reduced by loss of *ntc* and increased by its overexpression.

Interestingly, while we have shown that *ntc* overexpression is sufficient to induce basal mitophagy, independently of *Pink1/parkin*, and it is able to rescue *parkin* mutant phenotypes, curiously, it is not able to rescue *Pink1* phenotypes. As forced overexpression of *ntc* increases basal ubiquitination, it follows that already high levels of substrate for Pink1 circumvents the need for parkin ubiquitination (hence, why *ntc* overexpression can substitute for loss of *parkin*) when damage-induced mitophagy is required. However, despite high levels of latent ubiquitination, this is not sufficient to trigger damage-induced mitophagy in the absence of Pink1-mediated phosphorylation (hence, why *ntc* overexpression cannot rescue *Pink1* mutants). These findings further underscore the mechanistic and functional differences between basal and damage-induced mitophagy.

In summary, we propose a model (Fig. 8) in which FBXO7/ntc acts to prime OMM proteins with ubiquitin counteracted by USP30. This provides a key regulatory checkpoint in quality control of mitochondrial protein import. It is likely that occasional defects in import or protein folding may lead to an increase of Ub above threshold that provokes basal mitophagy. However, when the need arises this population of latent Ub could subsequently be phosphorylated (and amplified) to trigger selective degradation upon specific stimulation. Although more studies are required to understand the interplay between FBXO7/ntc, USP30, Pink1 and parkin, this study provides a foundation to elucidate further the interplay between these mechanisms of mitochondrial quality control and reinforces its potential as a therapeutic target.

Materials and Methods

Drosophila stocks and procedures

Drosophila were raised under standard conditions in a temperature-controlled incubator with a 12h:12h light:dark cycle at 25 °C and 65 % relative humidity, on food consisting of agar, cornmeal, molasses, propionic acid and yeast. *ntc*^{ms771}, *UAS-ntc* and *PBac{WH}CG10855*^{f07259} strains were kindly provided by H. Steller. *park*^{25} mutants

and *UAS-parkin*$_{C2}$ (Greene et al., 2003), *UAS-FBXO7* (Burchell et al., 2013), and *UAS-mito-QC* lines (Lee et al., 2018) have been previously described. *Pink1*^{B9} mutants (Park et al., 2006) were provided by J. Chung (KAIST). *UAS-Mul1* and *Mul1*^{A6} mutants were kindly provided by Ming Guo. *UAS-USP30* lines were kindly provided by Ugo Mayor. *UAS-USP30* RNAi (NIG-Fly 3016R[II]) was obtained from the NIG-Fly collection. The following strains were obtained from Bloomington *Drosophila* Stock Center (BDSC, RRID:SCR_006457): *w*^{1118} (RRID:BDSC_6326), *da-GAL4* (RRID:BDSC_55850), *nSyb-GAL4* (RRID:BDSC_51635), *GMR*-GAL4 (RRID:BDSC_1104), *Mef2*-GAL4 (RRID:BDSC_27390), *Act*-GAL4 (RRID:BDSC_25374), *Atg8a* [KG07569] *(Atg8a*$^{-/-}$*)* (RRID:BDSC_14639), UAS-GFP-mCherry-Atg8a (RRID:BDSC_37749) and *Df(3L)Exel6097* (RRID:BDSC_7576). *UAS-lacZ* was obtained from FlyORF (RRID: FlyBase_FBst0503118). The following strains were obtained from Vienna Drosophila Research Centre (VDRC): *UAS-LacZ*^{RNAi} (v51446), *UAS-March5* RNAi KK (v105711) and *UAS-March5* RNAi GD(v33309). *UAS-MQC*^{matrix} and *UAS-March5* lines were generated as follows: *MQC*^{matrix} mCherry-GFP was amplified from *UAS-mito-QC* and cloned in-frame with the mitochondrial targeting sequence from hCOX8A into pUAST.attB, and inserted in attP40 and attP16 sites; while for *March5* (*CG9855*), full length cDNA was cloned into pUAST vector and transgenesis performed by random insertion. A full description of the genotypes used in this study is shown in Supplementary table 1.

Locomotor and lifespan assays

For locomotor assays, climbing (negative geotaxis assay) was assessed as previously described, with minor modifications (Greene et al., 2003). For lifespan experiments flies were grown under identical conditions at low-density. Progeny were collected under very light anaesthesia and kept in tubes of approximately 20 males each. Flies were transferred every 2-3 days to fresh tubes with normal food for normal lifespan and tubes with 10 mM paraquat in a filter paper for the oxidative stress lifespan. The number of dead flies was recorded on each transfer. Percent of survival was calculated at the end of the experiment after correcting for any accidental loss.

Histology of adult thoraces

Thoraces were prepared from 5-day-old adult flies and treated as previously described (Greene et al., 2003). Semi-thin sections were then taken and stained with Toluidine blue, while ultra-thin sections were examined using a FEI Tecnai G2 Spirit 120KV transmission electron-microscope.

Light microscopy imaging and scanning electron microscopy of *Drosophila* eye

Light microscopy imaging was assessed using a Nikon motorized SMZ stereo zoom microscope fitted with 1x Apo lens. Extended focus images were then generated using Nikon Elements software, using the same settings for all the genotypes. Flies were anaesthetised with CO2 during the process. Scanning electron microscopy (SEM) was performed according to a standard protocol (Sullivan, 2000). All animals of a given genotype displayed essentially identical phenotypes and randomly selected representative images are shown. Images were taken using a SEM microscope (Philips XL-20 SEM).

Immunohistochemistry and sample preparation

Drosophila brains were dissected from 30-day-old flies and immune-stained with anti-tyrosine hydroxylase (Immunostar Inc. #22491) as described previously (Whitworth et al., 2005). Brains were imaged with an Olympus FV1000 confocal with SIM-scanner on a BX61 upright microscope. Tyrosine hydroxylase-positive neurons were counted under blinded conditions. For immunostaining, adult flight muscles were dissected in PBS and fixed in 4% formaldehyde for 30 min, permeabilized in 0.3% Triton X-100 for 30 min, and blocked with 0.3% Triton X-100 plus 1% bovine serum albumin in PBS for 1 h at RT. Tissues were incubated with ATP5A antibody (Abcam Cat# ab14748, RRID:AB_301447; 1:500), diluted in 0.3% Triton X-100 plus 1% bovine serum albumin in PBS overnight at 4°C, then rinsed 3 times 10 min with 0.3% Triton X-100 in PBS, and incubated with the appropriate fluorescent secondary antibodies overnight at 4°C. The tissues were washed 3 times in PBS and mounted on slides using Prolong Diamond Antifade mounting medium (Thermo Fischer Scientific) and image next day. For mitolysosome analysis of mito-QC and MQC^{matrix}, tissues were dissected and treated as previously described (Lee et al., 2018).

Mitochondrial morphology in larval brain

Third instar larvae overexpressing *UAS-mitoGFP* with the pan-neuronal driver nSyb-GAL4 were dissected in PBS and fixed in 4% formaldehyde for 30 min. The tissues were washed 3 times in PBS and mounted on slides using Prolong Diamond Antifade mounting medium (Thermo Fischer Scientific) and image next day in a Zeiss LSM880 confocal microscope (63x / 1.6NA).

ATP levels

The ATP assay was performed as described previously (Pogson et al., 2014). Briefly, five male flies of the indicated age for each genotype were homogenized in 100 μL 6M

guanidine-Tris/EDTA extraction buffer and subjected to rapid freezing in liquid nitrogen. Homogenates were diluted 1/100 with the extraction buffer and mixed with the luminescent solution (CellTiter-Glo Luminescent Cell Viability Assay (Promega, RRID:SCR_006724)). Luminescence was measured with a SpectraMax Gemini XPS luminometer (Molecular Devices). The average luminescent signal from technical triplicates was expressed relative to protein levels, quantified using the DC Protein Assay kit (Bio-Rad Laboratories, RRID:SCR_008426). Data from 2-4 independent experiments were averaged and the luminescence expressed as a percentage of the control.

Respirometry

Mitochondrial respiration was assayed at 30 °C by high-resolution respirometry using an Oxygraph-2k high-resolution respirometer (OROBOROS Instruments) using a chamber volume set to 2 mL. Calibration with the air-saturated medium was performed daily. Data acquisition and analysis were carried out using Datlab software (OROBOROS Instruments). Five flies per genotype were homogenised in Respiration Buffer [120 mM sucrose, 50 mM KCl, 20 mM Tris–HCl, 4 mM KH_2PO_4, 2 mM $MgCl_2$, and 1 mM EGTA, 1 g L^{-1} fatty acid-free BSA, pH 7.2]. For coupled (state 3) assays, complex I-linked respiration was measured at saturating concentrations of malate (2 mM), glutamate (10 mM), L-proline (10 mM) and adenosine diphosphate (ADP, 2.5 mM). Complex II-linked respiration was assayed in Respiration Buffer supplemented with 0.15 μM rotenone, 10 mM succinate and 2.5 mM ADP. Respiration was expressed as oxygen consumed per fly. Flies' weight was equal in all genotypes tested.

Image analysis and quantification of mitolysosomes

Analysis of mitolysosomes was done as previously described (Lee et al., 2018). Briefly, spinning disk microscopy–generated images from dissected larval brains or adult thoraces were processed using Imaris (version 9.0.2) analysis software (BitPlane; RRID:SCR_007370) to identify and count individual red-only puncta. The GFP and mCherry signals were adjusted to reduce background noise and retain only the distinct mitochondria network and red puncta, respectively. A surface rendered 3D structure corresponding to the mitochondria network was generated using the GFP signal. This volume was subtracted from the red channel to retain the mCherry signal that did not colocalize with the GFP-labelled mitochondria network. The mitolysosomes puncta were selected according to their intensity and an estimated size of 0.5 μm diameter, previously measured with Imaris. Additionally, the puncta were filtered with a minimum

size cut off of 0.2 μm diameter. The remaining puncta were counted as the number of mitolysosomes. Larval CNS soma were analysed individually where discrete cells could be distinguished. The mean number of mitolysosomes per cell was calculated per animal. Data points in the quantification charts show mean mitolysosomes per cell for individual animals, where $n \geq 6$ animals for each condition.

Analysis and quantification of autolysosomes using the GFP-mCherry-Atg8a traffic light reporter.

Third instar larval brains were dissected in phosphate buffered saline (PBS) and fixed with 4 % formaldehyde (FA) pH 7 (Thermo Scientific)/PBS for 20 minutes at room temperature. Samples were then washed in PBS followed by water to remove salts. Prolong antifade mounting media (Thermo Scientific) was used to mount the samples and imaged the day after. Confocal images, acquired with a Zeiss LSM880 microscope with the 63x/1.46 NA oil, were processed using FIJI (Image J). The quantification of autolysosomes was performed using FIJI (Image J) with the 3D Objects Counter Plugin. An area of interest was selected by choosing 6-10 cells per image. The threshold was based on matching the mask with the fluorescence. All puncta larger than 0.049 μm^3 was considered an autolysosome. Data points in the quantification charts show mean mitolysosomes per cell for individual animals, where $n \geq 3$ animals for each condition.

Mitochondrial enrichment by differential centrifugation

All steps were performed on ice or at 4 °C. For immunoblotting analysis and biochemical fractionation from small numbers of flies (10-30), a modified mitochondrial enrichment procedure was performed. Flies were prepared either fresh or after flash-freezing in liquid nitrogen, with all direct comparisons performed with flies that were prepared in the same manner. Flies were transferred into a Dounce homogeniser containing 700 μL Solution A (70 mM sucrose, 20 mM HEPES pH 7.6, 220 mM mannitol, 1 mM EDTA) containing cOmplete protease inhibitors (Roche) and PhosSTOP phosphatase inhibitors (Roche), and manually homogenised with 50 strokes of a pestle. The homogenate was transferred to an Eppendorf tube, a further 500 μl of Solution A was added to the homogeniser and the sample was homogenised with a further 10 strokes. The homogenates were pooled and incubated for 30 minutes, then centrifuged for 5 minutes at 800 x g. The supernatant (containing mitochondria) was transferred to a new tube and clarified twice by centrifugation for 5 minutes at 1,000 x g. The clarified supernatant was then centrifuged for 10 minutes at 10,000 x g and the post-mitochondrial supernatant was discarded and the pellet retained for

analysis. The mitochondrial pellet was washed once in Solution A containing only protease inhibitors, and then once in Solution A without inhibitors. The washed mitochondrial pellet was resuspended in 50 to 200 µL Sucrose Storage Buffer, the protein content determined by BCA assay (Thermo Pierce), and stored at -80 °C until needed.

Antibodies and dyes

The following mouse antibodies were used for immunoblotting (WB) in this study: ATP5A (Abcam, ab14748, 1:10000), Ubiquitin (clone P4D1, Cell Signalling Technology, 3936, 1:1000). The following rabbit antibodies were used in this study: pS65-Ub (Cell Signalling Technologies, 62802S, 1:1000), Marf ((Ziviani et al., 2010), 1:1000), GABARAP/Atg8a (Abcam ab109364, 1:1000), ref(2)P/p62 (Abcam ab178440, 1:1000). The following secondary antibodies were used: sheep anti-mouse (HRP-conjugated, GE Healthcare, NXA931V, 1:10000), donkey anti-rabbit (HRP-conjugated, GE Healthcare, NA934V, 1:10000).

Whole-animal lysis and immunoblotting

For the analysis of whole cell lysates by immunoblot, 180 µL cold RIPA buffer (150 mM NaCl, 1% (v/v) NP-40, 0.5 % (w/v) sodium deoxycholate, 0.1% (w/v) SDS, 50 mM Tris pH 7.4), supplemented with cOmplete protease inhibitors, was added to 2 mL tubes containing 1.4 mm ceramic beads (Fisherbrand 15555799). Animals (5 to 20 per replicate) were harvested and stored on ice or flash-frozen in liquid N_2, with all direct comparisons performed with flies that were harvested in the same manner. The flies were added to the tubes containing RIPA buffer and lysed using a Minilys homogeniser (Bertin Instruments) with the following settings: maximum speed, 10 seconds on, 10 seconds on ice, for a total of three cycles. After lysis, samples were returned to ice for 10 minutes then centrifuged 5 minutes at 21,000 x g, 4 °C. 90 µL supernatant was transferred to a fresh Eppendorf tube and centrifuged a further 10 minutes at 21,000 x g. 50 µL supernatant was then transferred to a fresh Eppendorf tube and the protein content determined by BCA assay as above. 30 µg total protein was then diluted in Laemli Sample Buffer (Bio-Rad, 1610747) and analysed by SDS-PAGE using Mini-PROTEAN TGX Gels 4-20% (Bio-Rad, 4561093). For the analysis of mitochondria-enriched fractions, 30 µg mitochondrial protein was aliquoted into a tube, centrifuged 10 minutes at 16,000 x g, the supernatant removed and the pellet resuspended in Laemli Sample Buffer (Bio-Rad, 1610747) to SDS-PAGE analysis as above. Gels were transferred onto pre-cut and soaked PVDF membranes (1704156, BioRad) using the BioRad Transblot Turbo transfer system, and blots were immediately stained with No-

Stain™ Protein Labeling Reagent (Invitrogen, A44449) where indicated, according to the manufacturer's instructions. Fluorescence intensity was measured using a BioRad Chemidoc MP using the IR680 setting. Blots were then washed by gentle shaking 3 times for 5 minutes in PBS containing 0.1% (v/v) Tween-20 (PBST), and blocked by incubation with PBST containing 3 % (w/v) BSA for 1 hour. Blots were washed a further 3 times as above then incubated at 4 °C overnight with primary antibodies in PBST containing 3 % (w/v) BSA. A further 3 washes were performed then the blots were incubated for one hour in secondary antibodies made up in PBST containing 3 % (w/v) BSA. Blots were then washed twice in PBST and once in PBS prior to incubation with ECL reagent (GE Healthcare, RPN2109). Blots were imaged using the BioRad Chemidoc MP using exposure settings to minimise overexposure. Image analysis was performed using FIJI (Image J) and images were exported as TIFF files for publication.

ARPE-19-MQC cells

ARPE-19-MQC-FIS1 cells were used to assess mitophagy in a human cell model. Briefly, cells were transfected in reverse with RNAiMax (13778075, Thermo Fisher Scientific) and non-targeting control siRNA (ON-TARGETplus Non-targeting Control Pool, D-001810-10-20, Horizon Discovery) or FBXO7 siRNA (ON-TARGETplus Human FBXO7 siRNA, L-013606-00-0010, Horizon Discovery). After 48h knockdown cells were seeded into and ibidi dish (IB-81156) Thistle Scientific Ltd), and after 72h cells were imaged live by a spinning disk microscope and generated images were processed using Imaris as previously described.

Statistical analysis

Data are reported as mean ± SEM or mean ± 95% CI as indicated in figure legends, and the n numbers of distinct biological replicates are shown in each graph. For statistical analyses of lifespan experiments, a log rank (Mantel-Cox) test was used. For behavioural analyses, a Kruskal-Wallis nonparametric test with Dunn's post-hoc correction for multiple comparisons was used. Where multiple groups were compared, statistical significance was calculated by one-way ANOVA with Bonferroni post-test correction for multiple samples. This test was applied to dopaminergic neuron analysis and mitophagy where more than two groups were compared. For Ub and pS65-Ub abundance an Ordinary one-way ANOVA with Dunnett's correction for multiple comparisons was used. When only two groups were compared a Welsch's *t* test was used. The absence of statistical analysis in between any group reflects "no statistical significance". All the samples were collected and processed simultaneously and

therefore no randomization was appropriate. Unless otherwise indicated, all the acquisition of images and analysis was done in blind conditions. Statistical analyses were performed using GraphPad Prism 9 software (GraphPad Prism, RRID:SCR_002798). Statistical significance was represented in all cases as follows: * $P < 0.05$, ** $P < 0.01$, *** $P < 0.001$ and **** $P < 0.0001$.

Data Availability

All data needed to evaluate the conclusions in the paper are present in the paper and/or the Supplementary Material. This study includes no data deposited in external repositories.

Acknowledgements

We kindly thank Herman Steller for generously sharing the ntc lines, Ugo Mayor for the USP30 lines and Ian Ganley for the ARPE-19-MQC cells. We thank Roberta Tufi for performing the ATP assay, Wing Hei Au and Federica De Lazzari for comments on the manuscript, and all the members of the Whitworth's lab for discussions. **Funding**: This work is supported by MRC core funding (MC_UU_00028/6). A.M. is funded by the Basque Government Posdoctoral Fellowship. Stocks were obtained from the Bloomington *Drosophila* Stock Center which is supported by grant NIH P40OD018537.

Author contributions: A.S.M. conceived the project, designed the experiments, performed experimental work, analysed data, wrote the original draft, revised and edited the manuscript. A.M. conceived parts of the project, designed and performed some experimental work, analysed data and revised and edited the manuscript. A.J.W. conceived and supervised the project, wrote the original draft, revised and edited the manuscript. **Competing interests:** The authors declare that they have no competing interests. **Data and materials availability:** All data needed to evaluate the conclusions in the paper are present in the paper and/or the Supplementary Materials. Additional data related to this paper may be requested from the authors.

Figure Legends

Fig. 1 Nutcracker overexpression is able to rescue *parkin* but not *Pink1* mutants. (**A**) Climbing ability of 2 days old control and *parkin* mutants alone or with transgenic expression of *ntc* with the ubiquitous driver *da*-GAL4. Chart show mean ± 95% CI and n values. Kruskal-Wallis nonparametric test with Dunn's post-hoc correction for multiple comparisons; **** $P < 0.0001$. (**B**) Quantification of dopaminergic neurons (PPL1 cluster) in 30 days old control and *parkin* mutants alone or with transgenic expression of *ntc* with the ubiquitous driver *da*-GAL4. Data represented as means ± SEM; n shown in chart. One-way ANOVA with Bonferroni post-test correction; **** $P < 0.0001$. (**C**) Toluidine blue staining, and (**D**) transmission electron microscopy (TEM) analysis of thoraces from 2 days old control and *parkin* mutant alone or with transgenic expression of *ntc* with the ubiquitous driver *da*-GAL4. Scale bars; top = 200 µm, middle = 10 µm, bottom = 2 µm. (**E**) Western blot analysis from whole fly lysates of Marf steady state levels from 2 days old control and *parkin* mutants alone or with transgenic expression of *ntc* with the ubiquitous driver *da*-GAL4. (**F**) Climbing and (**G**) flight ability of 2 days old control and *Pink1* mutants alone or with transgenic expression of *ntc* with the ubiquitous driver *da*-GAL4. Chart show mean ± 95% CI; n shown in chart. Kruskal-Wallis nonparametric test with Dunn's post-hoc correction for multiple comparisons; **** $P < 0.0001$. (**H**) Western blot analysis from whole fly lysates of Marf steady state levels from 2 days old control and *Pink1* mutants alone or with transgenic expression of *ntc* with the ubiquitous driver *da*-GAL4. (**I**) Analysis of the compound eye by (top panels) light microscopy or (middle and bottom panels) scanning electron microscopy (SEM) of 2 days old control, overexpression of ntc, Pink1 or both combine using the *GMR*-GAL4 driver. Scale bars; top and middle = 100 µm, bottom = 50 µm.

Fig. 2 Loss of ntc has motor and lifespan deficits, no gross effect on mitochondria but increased sensitivity to oxidative stress.
Analysis of (**A**) climbing and (**B**) flight abilities of 2 days old control and *ntc* mutants alone or with transgenic expression of *ntc* with the ubiquitous driver *da*-GAL4. Chart show mean ± 95% CI and n values. Kruskal-Wallis nonparametric test with Dunn's post-hoc correction for multiple comparisons; ** $P < 0.01$, *** $P < 0.001$, **** $P < 0.0001$. (**C**) Lifespan assay of control and *ntc* mutants alone or with transgenic expression of *ntc* with the ubiquitous driver *da*-GAL4; n shown in chart. Log rank (Mantel-Cox) test; **** $P < 0.0001$. (**D**) Quantification of dopaminergic neurons (PPL1 cluster) in 10 days old control and *ntc* mutants alone. Data represented as means ± SEM; n shown in chart. One-way ANOVA with Bonferroni post-test correction. (**E**) (Top panel)

Immunohistochemistry with anti-ATP5A staining and (bottom panel) transmission electron microscopy of 2 days old adult thoraces from control and *ntc* mutants. Scale bars; top = 10 μm, bottom = 2 μm. (**F**) Mitochondrial morphology in motoneurons from the ventral nerve cord of third instar larvae in control and *ntc* mutants, overexpressing mito-GFP with the pan-neuronal driver *nSyb*-GAL4. (**G**) Oxygen consumption rate from complex I and complex II of 2 days old control and *ntc* mutants. Data represented as means ± SEM; n shown in chart. One-way ANOVA with Bonferroni post-test correction. (**H**) ATP levels of 2 days old control and *ntc* mutants alone or with transgenic expression of *ntc* with the ubiquitous driver *da*-GAL4. Data represented as means ± SEM; n shown in chart. One-way ANOVA with Bonferroni post-test correction; * $P < 0.05$, ** $P < 0.01$. (**I**) Lifespan assay of control and *ntc* mutants treated with 10 μM paraquat. n shown in chart. Log rank (Mantel-Cox) test; **** $P < 0.0001$.

Fig. 3 ntc affects basal mitophagy and counteracts USP30.

(**A**, **B**) Confocal microscopy analysis of the mito-QC reporter in larval CNS of control and *ntc* mutant alone or with transgenic expression of *ntc* with the pan-neuronal driver *nSyb*-GAL4. Mitolysosomes are evident as GFP-negative/mCherry-positive (red-only) puncta. n shown in chart. One-way ANOVA with Bonferroni post-test correction; ** $P < 0.01$. Scale bars = 10 μm. (**C**, **D**) Confocal microscopy analysis of the mito-QC reporter in larval CNS of control and transgenic expression of *ntc* with the pan-neuronal driver *nSyb*-GAL4. Mitolysosomes are evident as GFP-negative/mCherry-positive (red-only) puncta. n shown in chart. One-way ANOVA with Bonferroni post-test correction; *** $P < 0.001$. Scale bars = 10 μm. (**E**, **F**) Confocal microscopy analysis of the mito-QC reporter in larval CNS of control and knockdown of USP30 with the pan-neuronal driver *nSyb*-GAL4 alone or in combination with *ntc* mutant. Mitolysosomes are evident as GFP-negative/mCherry-positive (red-only) puncta. n shown in chart. One-way ANOVA with Bonferroni post-test correction; * $P < 0.05$, *** $P < 0.001$. Scale bars = 10 μm. (**G**) Climbing ability of 10 days old flies overexpressing USP30 alone or in combination with ntc or parkin with the ubiquitous driver *Act*-GAL4. Chart show mean ± 95% CI; n shown in chart. Kruskal-Wallis nonparametric test with Dunn's post-hoc correction for multiple comparisons; **** $P < 0.0001$.

Fig. 4 ntc regulates basal mitophagy in a parkin and Pink1 independent manner.

(**A**, **B**) Confocal microscopy analysis of the mito-QC reporter in larval CNS of control and *parkin* mutant alone or with transgenic expression of *ntc* with the pan-neuronal driver *nSyb*-GAL4. Mitolysosomes are evident as GFP-negative/mCherry-positive (red-only) puncta. n shown in chart. One-way ANOVA with Bonferroni post-test

correction; * $P < 0.05$, ** $P < 0.01$. Scale bars = 10 μm. (**C**, **D**) Confocal microscopy analysis of the mito-QC reporter in larval CNS of control and *Pink1* mutant alone or with transgenic expression of *ntc* with the pan-neuronal driver *nSyb*-GAL4. Mitolysosomes are evident as GFP-negative/mCherry-positive (red-only) puncta. n shown in chart. One-way ANOVA with Bonferroni post-test correction; * $P < 0.05$, ** $P < 0.01$. Scale bars = 10 μm.

Fig. 5 ntc is required for USP30 knockdown induced basal mitophagy in the absence of parkin or Pink1

(**A**, **B**) Confocal microscopy analysis of the mito-QC reporter in larval CNS of control, knockdown of USP30 with the pan-neuronal driver *nSyb*-GAL4 alone or in combination with *ntc* mutants in a *parkin* mutant background. Mitolysosomes are evident as GFP-negative/mCherry-positive (red-only) puncta. n shown in chart. One-way ANOVA with Bonferroni post-test correction; * $P < 0.05$, ** $P < 0.01$, *** $P < 0.001$. Scale bars = 10 μm. (**C**, **D**) Confocal microscopy analysis of the mito-QC reporter in larval CNS of control, knockdown of USP30 with the pan-neuronal driver *nSyb*-GAL4 alone or in combination with *ntc* mutants in a *Pink1* mutant background. Mitolysosomes are evident as GFP-negative/mCherry-positive (red-only) puncta. n shown in chart. One-way ANOVA with Bonferroni post-test correction; * $P < 0.05$, ** $P < 0.01$. Scale bars = 10 μm.

Fig. 6 Manipulating mitophagy by altering levels of USP30 or ntc do not have an effect on general autophagy.

(**A**, **B**) Representative western blot from whole fly lysates of Atg8a (non-lipidated) I and II (lipidated) in control, USP30 knockdown, ntc overexpression and *ntc* mutant with the ubiquitous driver *da*-GAL4. Data represented as means ± SD; n shown in chart. One-way ANOVA with Bonferroni post-test correction. (**C**, **D**) Representative western blot from whole fly lysates of ref(2)P/p62 in control, USP30 knockdown, ntc overexpression and *ntc* mutant with the ubiquitous driver *da*-GAL4. Data represented as means ± SD; n shown in chart. One-way ANOVA with Bonferroni post-test correction. (**E**, **F**) Confocal microscopy analysis and quantification of the red-only (autolysosomes) puncta per cell of larval CNS expressing the autophagy flux marker GFP-mCherry-Atg8a (red and green) in combination with USP30 knockdown, ntc overexpression and *ntc* mutant with the pan-neuronal driver *nSyb*-GAL4. Data represented as means ± SEM; n shown in chart. One-way ANOVA with Bonferroni post-test correction; Scale bars = 10 μm.

Fig. 7 Both ntc overexpression and USP30 depletion promote accumulation of ubiquitin in the mitochondria and are necessary for pS65-Ub formation.
(**A**) Representative western blot and quantification of (**B**) mitochondrial ubiquitin (anti-P4D1) in control, ntc overexpression and USP30 knockdown with the ubiquitous driver *da*-GAL4. Data represented as means ± SD; n shown in chart. One-way ANOVA with Bonferroni post-test correction; * $P < 0.05$, ** $P < 0.01$. (**C**, **D**) Representative western blot and quantification of mitochondrial pS65-Ub in *parkin* mutants, *ntc* mutants and the double *parkin-ntc* mutant. Data represented as means ± SD; n shown in chart. One-way ANOVA with Bonferroni post-test correction; * $P < 0.05$, **** $P < 0.0001$. (**E**, **F**) Representative western blot and quantification of mitochondrial pS65-Ub in control and *parkin* mutants alone or with the transgenic expression of ntc with the ubiquitous driver *da*-GAL4. Data represented as means ± SD; n shown in chart. One-way ANOVA with Bonferroni post-test correction; **** $P < 0.0001$.

Fig. 8 Proposed model for basal and damage-induced mitophagy regulated by ntc, USP30 and parkin.
FBXO7/ntc acts to prime OMM proteins with ubiquitin counteracted by USP30. This provides a key regulatory checkpoint in quality control of mitochondrial protein import. Occasional defects in import or protein folding may lead to a Ub threshold that provokes basal mitophagy. However, when the need arises this population of latent Ub could subsequently be phosphorylated and amplified by parkin to trigger selective degradation upon specific stimulation. Created with BioRender.com.

Supplementary figures

fig. S1 mito-QC reporter targeted to the mitochondrial matrix (MQC^{matrix}) reproduces the results observed with the mito-QC.
(**A**, **B**) Confocal microscopy analysis of the MQC^{matrix} reporter in larval CNS of control, *ntc* mutant, *ntc* overexpression and USP30 knockdown with the pan-neuronal driver *nSyb*-GAL4. Mitolysosomes are evident as GFP-negative/mCherry-positive (red-only) puncta. n shown in chart. One-way ANOVA with Bonferroni post-test correction; * $P < 0.05$. Scale bars = 10 μm.

fig. S2 FBXO7 affects basal mitophagy *in vivo Drosophila* neurons and in a human cell line.

(**A**, **B**) Confocal microscopy analysis of the mito-QC reporter in larval CNS of control and the transgenic expression of *FBXO7* with the pan-neuronal driver *nSyb*-GAL4. Mitolysosomes are evident as GFP-negative/mCherry-positive (red-only) puncta; n shown in chart. One-way ANOVA with Bonferroni post-test correction; *** $P < 0.001$. Scale bars = 10 μm. (**C**) Western blot analysis of the knockdown of FBXO7 in human ARPE-19 cells expressing the mito-QC reporter. Arrow shows FBXO7 band; * shows none specific band. (**D**, **E**) Confocal microscopy analysis of the mito-QC reporter in ARPE-19 human cell line of control siRNA and FBXO7 siRNA. Mitolysosomes are evident as GFP-negative/mCherry-positive (red-only) puncta. n shown in chart. Two-tailed *t* test; ** $P < 0.01$. Scale bars = 10 μm.

fig. S3 USP30 but neither March5 nor MUL1 can modulate mitophagy *in vivo*.
(**A**, **B**) Confocal microscopy analysis of the mito-QC reporter in 2 days old adult thoraces of control and USP30 knockdown with the muscular driver *Mef2*-GAL4. Mitolysosomes are evident as GFP-negative/mCherry-positive (red-only) puncta. n shown in chart. Two-tailed *t* test; * $P < 0.05$. Scale bars = 10 μm. (**C**) Climbing ability of 10 days old flies overexpressing USP30 alone or in combination with parkin, March5 or Mul1 with the ubiquitous driver *Act*-GAL4. Chart show mean ± 95% CI and n values. Kruskal-Wallis nonparametric test with Dunn's post-hoc correction for multiple comparisons; **** $P < 0.0001$. (**D**, **E**) Confocal microscopy analysis of the mito-QC reporter in larval CNS of control and parkin overexpression with the pan-neuronal driver *nSyb*-GAL4. Mitolysosomes are evident as GFP-negative/mCherry-positive (red-only) puncta; n shown in chart. Two-tailed *t* test. Scale bars = 10 μm. (**F**, **G**) Confocal microscopy analysis of the mito-QC reporter in larval CNS of control and *Mul1* mutant. Mitolysosomes are evident as GFP-negative/mCherry-positive (red-only) puncta. n shown in chart. Two-tailed *t* test. Scale bars = 10 μm (**H**, **I**) Confocal microscopy analysis of the mito-QC reporter in larval CNS of control and March5 knockdowns with the pan-neuronal driver *nSyb*-GAL4. Mitolysosomes are evident as GFP-negative/mCherry-positive (red-only) puncta. n shown in chart. Two-tailed *t* test. Scale bars = 10 μm.

fig. S4 Increase in mitophagy levels requires the critical autophagy factor Atg8.
(**A**, **B**) Confocal microscopy analysis of the mito-QC reporter in larval CNS of control, knockdown of USP30, overexpression of ntc and *ntc* mutant in the *Atg8a* mutant background with the pan-neuronal driver *nSyb*-GAL4. Mitolysosomes are evident as GFP-negative/mCherry-positive (red-only) puncta. n shown in chart. One-way ANOVA with Bonferroni post-test correction; * $P < 0.05$, *** $P < 0.001$. Scale bars = 10 μm. (**C**,

D) Confocal microscopy analysis of the mito-QC reporter in larval CNS of control and *parkin* mutant alone or with the USP30 knockdown in the presence or absence of *Atg8a*, with the pan-neuronal driver *nSyb*-GAL4. Mitolysosomes are evident as GFP-negative/mCherry-positive (red-only) puncta; n shown in chart. One-way ANOVA with Bonferroni post-test correction; * $P < 0.05$, ** $P < 0.01$, **** $P < 0.0001$. Scale bars = 10 µm.

References

Allen, G.F., R. Toth, J. James, and I.G. Ganley. 2013. Loss of iron triggers PINK1/Parkin-independent mitophagy. *EMBO Rep*. 14:1127-1135.

Ashrafi, G., and T.L. Schwarz. 2013. The pathways of mitophagy for quality control and clearance of mitochondria. *Cell Death Differ*. 20:31-42.

Bader, M., E. Arama, and H. Steller. 2010. A novel F-box protein is required for caspase activation during cellular remodeling in Drosophila. *Development*. 137:1679-1688.

Bader, M., S. Benjamin, O.L. Wapinski, D.M. Smith, A.L. Goldberg, and H. Steller. 2011. A conserved F box regulatory complex controls proteasome activity in Drosophila. *Cell*. 145:371-382.

Bingol, B., and M. Sheng. 2016. Mechanisms of mitophagy: PINK1, Parkin, USP30 and beyond. *Free Radic Biol Med*. 100:210-222.

Bingol, B., J.S. Tea, L. Phu, M. Reichelt, C.E. Bakalarski, Q. Song, O. Foreman, D.S. Kirkpatrick, and M. Sheng. 2014. The mitochondrial deubiquitinase USP30 opposes parkin-mediated mitophagy. *Nature*. 510:370-375.

Burchell, V.S., D.E. Nelson, A. Sanchez-Martinez, M. Delgado-Camprubi, R.M. Ivatt, J.H. Pogson, S.J. Randle, S. Wray, P.A. Lewis, H. Houlden, A.Y. Abramov, J. Hardy, N.W. Wood, A.J. Whitworth, H. Laman, and H. Plun-Favreau. 2013. The Parkinson's disease-linked proteins Fbxo7 and Parkin interact to mediate mitophagy. *Nat Neurosci*. 16:1257-1265.

Chen, Z., L. Liu, Q. Cheng, Y. Li, H. Wu, W. Zhang, Y. Wang, S.A. Sehgal, S. Siraj, X. Wang, J. Wang, Y. Zhu, and Q. Chen. 2017. Mitochondrial E3 ligase MARCH5 regulates FUNDC1 to fine-tune hypoxic mitophagy. *EMBO Rep*. 18:495-509.

Clark, I.E., M.W. Dodson, C. Jiang, J.H. Cao, J.R. Huh, J.H. Seol, S.J. Yoo, B.A. Hay, and M. Guo. 2006. Drosophila pink1 is required for mitochondrial function and interacts genetically with parkin. *Nature*. 441:1162-1166.

Cornelissen, T., P. Verstreken, and W. Vandenberghe. 2018. Imaging mitophagy in the fruit fly. *Autophagy*. 14:1656-1657.

Cunningham, C.N., J.M. Baughman, L. Phu, J.S. Tea, C. Yu, M. Coons, D.S. Kirkpatrick, B. Bingol, and J.E. Corn. 2015. USP30 and parkin homeostatically regulate atypical ubiquitin chains on mitochondria. *Nat Cell Biol*. 17:160-169.

Di Fonzo, A., M.C. Dekker, P. Montagna, A. Baruzzi, E.H. Yonova, L. Correia Guedes, A. Szczerbinska, T. Zhao, L.O. Dubbel-Hulsman, C.H. Wouters, E. de Graaff, W.J. Oyen, E.J. Simons, G.J. Breedveld, B.A. Oostra, M.W. Horstink, and V. Bonifati. 2009. FBXO7 mutations cause autosomal recessive, early-onset parkinsonian-pyramidal syndrome. *Neurology*. 72:240-245.

Gersch, M., C. Gladkova, A.F. Schubert, M.A. Michel, S. Maslen, and D. Komander. 2017. Mechanism and regulation of the Lys6-selective deubiquitinase USP30. *Nat Struct Mol Biol*. 24:920-930.

Gladkova, C., S.L. Maslen, J.M. Skehel, and D. Komander. 2018. Mechanism of parkin activation by PINK1. *Nature*. 559:410-414.

Greene, J.C., A.J. Whitworth, I. Kuo, L.A. Andrews, M.B. Feany, and L.J. Pallanck. 2003. Mitochondrial pathology and apoptotic muscle degeneration in Drosophila parkin mutants. *Proc Natl Acad Sci U S A*. 100:4078-4083.

Hsu, J.M., Y.C. Lee, C.T. Yu, and C.Y. Huang. 2004. Fbx7 functions in the SCF complex regulating Cdk1-cyclin B-phosphorylated hepatoma up-regulated protein (HURP) proteolysis by a proline-rich region. *J Biol Chem*. 279:32592-32602.

Jipa, A., V. Vedelek, Z. Merenyi, A. Urmosi, S. Takats, A.L. Kovacs, G.V. Horvath, R. Sinka, and G. Juhasz. 2021. Analysis of Drosophila Atg8 proteins reveals multiple lipidation-independent roles. *Autophagy*. 17:2565-2575.

Kim, Y.Y., J.H. Um, J.H. Yoon, H. Kim, D.Y. Lee, Y.J. Lee, H.J. Jee, Y.M. Kim, J.S. Jang, Y.G. Jang, J. Chung, H.T. Park, T. Finkel, H. Koh, and J. Yun. 2019. Assessment of mitophagy in mt-Keima Drosophila revealed an essential role of the PINK1-Parkin pathway in mitophagy induction in vivo. *FASEB J*. 33:9742-9751.

Kirk, R., H. Laman, P.P. Knowles, J. Murray-Rust, M. Lomonosov, K. Meziane el, and N.Q. McDonald. 2008. Structure of a conserved dimerization domain within the F-box protein Fbxo7 and the PI31 proteasome inhibitor. *J Biol Chem*. 283:22325-22335.

Koyano, F., K. Yamano, H. Kosako, Y. Kimura, M. Kimura, Y. Fujiki, K. Tanaka, and N. Matsuda. 2019. Parkin-mediated ubiquitylation redistributes MITOL/March5 from mitochondria to peroxisomes. *EMBO Rep*. 20:e47728.

Lazarou, M., M. McKenzie, A. Ohtake, D.R. Thorburn, and M.T. Ryan. 2007. Analysis of the assembly profiles for mitochondrial- and nuclear-DNA-encoded subunits into complex I. *Mol Cell Biol*. 27:4228-4237.

Lazarou, M., D.A. Sliter, L.A. Kane, S.A. Sarraf, C. Wang, J.L. Burman, D.P. Sideris, A.I. Fogel, and R.J. Youle. 2015. The ubiquitin kinase PINK1 recruits autophagy receptors to induce mitophagy. *Nature*. 524:309-314.

Lee, J.J., A. Sanchez-Martinez, A. Martinez Zarate, C. Beninca, U. Mayor, M.J. Clague, and A.J. Whitworth. 2018. Basal mitophagy is widespread in Drosophila but minimally affected by loss of Pink1 or parkin. *J Cell Biol*. 217:1613-1622.

Liang, J.R., A. Martinez, J.D. Lane, U. Mayor, M.J. Clague, and S. Urbe. 2015. USP30 deubiquitylates mitochondrial Parkin substrates and restricts apoptotic cell death. *EMBO Rep*. 16:618-627.

Lorincz, P., C. Mauvezin, and G. Juhasz. 2017. Exploring Autophagy in Drosophila. *Cells*. 6.

Low, P., A. Varga, K. Pircs, P. Nagy, Z. Szatmari, M. Sass, and G. Juhasz. 2013. Impaired proteasomal degradation enhances autophagy via hypoxia signaling in Drosophila. *BMC Cell Biol*. 14:29.

Malik, B.R., V.K. Godena, and A.J. Whitworth. 2015. VPS35 pathogenic mutations confer no dominant toxicity but partial loss of function in Drosophila and genetically interact with parkin. *Hum Mol Genet*. 24:6106-6117.

Marcassa, E., A. Kallinos, J. Jardine, E.V. Rusilowicz-Jones, A. Martinez, S. Kuehl, M. Islinger, M.J. Clague, and S. Urbe. 2018. Dual role of USP30 in controlling basal pexophagy and mitophagy. *EMBO Rep*. 19.

Mauvezin, C., C. Ayala, C.R. Braden, J. Kim, and T.P. Neufeld. 2014. Assays to monitor autophagy in Drosophila. *Methods*. 68:134-139.

McWilliams, T.G., A.R. Prescott, L. Montava-Garriga, G. Ball, F. Singh, E. Barini, M.M.K. Muqit, S.P. Brooks, and I.G. Ganley. 2018. Basal Mitophagy Occurs Independently of PINK1 in Mouse Tissues of High Metabolic Demand. *Cell Metab*. 27:439-449 e435.

Meulener, M., A.J. Whitworth, C.E. Armstrong-Gold, P. Rizzu, P. Heutink, P.D. Wes, L.J. Pallanck, and N.M. Bonini. 2005. Drosophila DJ-1 mutants are selectively sensitive to environmental toxins associated with Parkinson's disease. *Curr Biol*. 15:1572-1577.

Montava-Garriga, L., F. Singh, G. Ball, and I.G. Ganley. 2020. Semi-automated quantitation of mitophagy in cells and tissues. *Mech Ageing Dev*. 185:111196.

Nagy, P., M. Karpati, A. Varga, K. Pircs, Z. Venkei, S. Takats, K. Varga, B. Erdi, K. Hegedus, and G. Juhasz. 2014. Atg17/FIP200 localizes to perilysosomal Ref(2)P aggregates and promotes autophagy by activation of Atg1 in Drosophila. *Autophagy*. 10:453-467.

Nguyen, T.N., B.S. Padman, J. Usher, V. Oorschot, G. Ramm, and M. Lazarou. 2016. Atg8 family LC3/GABARAP proteins are crucial for autophagosome-lysosome fusion but not autophagosome formation during PINK1/Parkin mitophagy and starvation. *J Cell Biol*. 215:857-874.

Okatsu, K., M. Kimura, T. Oka, K. Tanaka, and N. Matsuda. 2015a. Unconventional PINK1 localization to the outer membrane of depolarized mitochondria drives Parkin recruitment. *J Cell Sci*. 128:964-978.

Okatsu, K., F. Koyano, M. Kimura, H. Kosako, Y. Saeki, K. Tanaka, and N. Matsuda. 2015b. Phosphorylated ubiquitin chain is the genuine Parkin receptor. *J Cell Biol*. 209:111-128.

Ordureau, A., J.M. Heo, D.M. Duda, J.A. Paulo, J.L. Olszewski, D. Yanishevski, J. Rinehart, B.A. Schulman, and J.W. Harper. 2015. Defining roles of PARKIN and ubiquitin phosphorylation by PINK1 in mitochondrial quality control using a ubiquitin replacement strategy. *Proc Natl Acad Sci U S A*. 112:6637-6642.

Ordureau, A., J.A. Paulo, J. Zhang, H. An, K.N. Swatek, J.R. Cannon, Q. Wan, D. Komander, and J.W. Harper. 2020. Global Landscape and Dynamics of Parkin and USP30-Dependent Ubiquitylomes in iNeurons during Mitophagic Signaling. *Mol Cell*. 77:1124-1142 e1110.

Ordureau, A., S.A. Sarraf, D.M. Duda, J.M. Heo, M.P. Jedrychowski, V.O. Sviderskiy, J.L. Olszewski, J.T. Koerber, T. Xie, S.A. Beausoleil, J.A. Wells, S.P. Gygi, B.A. Schulman, and J.W. Harper. 2014. Quantitative proteomics reveal a feedforward mechanism for mitochondrial PARKIN translocation and ubiquitin chain synthesis. *Mol Cell*. 56:360-375.

Pan, W., Y. Wang, X. Bai, Y. Yin, L. Dai, H. Zhou, Q. Wu, and Y. Wang. 2021. Deubiquitinating enzyme USP30 negatively regulates mitophagy and accelerates myocardial cell senescence through antagonism of Parkin. *Cell Death Discov*. 7:187.

Park, J., S.B. Lee, S. Lee, Y. Kim, S. Song, S. Kim, E. Bae, J. Kim, M. Shong, J.M. Kim, and J. Chung. 2006. Mitochondrial dysfunction in Drosophila PINK1 mutants is complemented by parkin. *Nature*. 441:1157-1161.

Phu, L., C.M. Rose, J.S. Tea, C.E. Wall, E. Verschueren, T.K. Cheung, D.S. Kirkpatrick, and B. Bingol. 2020. Dynamic Regulation of Mitochondrial Import by the Ubiquitin System. *Mol Cell*. 77:1107-1123 e1110.

Pickles, S., P. Vigie, and R.J. Youle. 2018. Mitophagy and Quality Control Mechanisms in Mitochondrial Maintenance. *Curr Biol*. 28:R170-R185.

Pickrell, A.M., and R.J. Youle. 2015. The roles of PINK1, parkin, and mitochondrial fidelity in Parkinson's disease. *Neuron*. 85:257-273.

Pogson, J.H., R.M. Ivatt, A. Sanchez-Martinez, R. Tufi, E. Wilson, H. Mortiboys, and A.J. Whitworth. 2014. The complex I subunit NDUFA10 selectively rescues Drosophila pink1 mutants through a mechanism independent of mitophagy. *PLoS Genet*. 10:e1004815.

Poole, A.C., R.E. Thomas, L.A. Andrews, H.M. McBride, A.J. Whitworth, and L.J. Pallanck. 2008. The PINK1/Parkin pathway regulates mitochondrial morphology. *Proc Natl Acad Sci U S A*. 105:1638-1643.

Riparbelli, M.G., and G. Callaini. 2007. The Drosophila parkin homologue is required for normal mitochondrial dynamics during spermiogenesis. *Dev Biol*. 303:108-120.

Rojansky, R., M.Y. Cha, and D.C. Chan. 2016. Elimination of paternal mitochondria in mouse embryos occurs through autophagic degradation dependent on PARKIN and MUL1. *Elife*. 5.

Rusilowicz-Jones, E.V., J. Jardine, A. Kallinos, A. Pinto-Fernandez, F. Guenther, M. Giurrandino, F.G. Barone, K. McCarron, C.J. Burke, A. Murad, A. Martinez, E. Marcassa, M. Gersch, A.J. Buckmelter, K.J. Kayser-Bricker, F. Lamoliatte, A. Gajbhiye, S. Davis, H.C. Scott, E. Murphy, K. England, H. Mortiboys, D. Komander, M. Trost, B.M. Kessler, S. Ioannidis, M.K. Ahlijanian, S. Urbe, and

M.J. Clague. 2020. USP30 sets a trigger threshold for PINK1-PARKIN amplification of mitochondrial ubiquitylation. *Life Sci Alliance*. 3.

Sauve, V., G. Sung, N. Soya, G. Kozlov, N. Blaimschein, L.S. Miotto, J.F. Trempe, G.L. Lukacs, and K. Gehring. 2018. Mechanism of parkin activation by phosphorylation. *Nat Struct Mol Biol*. 25:623-630.

Shen, J.L., T.M. Fortier, R. Wang, and E.H. Baehrecke. 2021. Vps13D functions in a Pink1-dependent and Parkin-independent mitophagy pathway. *J Cell Biol*. 220.

Skowyra, D., K.L. Craig, M. Tyers, S.J. Elledge, and J.W. Harper. 1997. F-box proteins are receptors that recruit phosphorylated substrates to the SCF ubiquitin-ligase complex. *Cell*. 91:209-219.

Song, S., S. Jang, J. Park, S. Bang, S. Choi, K.Y. Kwon, X. Zhuang, E. Kim, and J. Chung. 2013. Characterization of PINK1 (PTEN-induced putative kinase 1) mutations associated with Parkinson disease in mammalian cells and Drosophila. *J Biol Chem*. 288:5660-5672.

Sullivan, W.A., M. ; Hawley, R. S. 2000. Drosophila protocols. *Cold Spring Harbor Laboratory Press*.

Teixeira, F.R., S.J. Randle, S.P. Patel, T.E. Mevissen, G. Zenkeviciute, T. Koide, D. Komander, and H. Laman. 2016. Gsk3beta and Tomm20 are substrates of the SCFFbxo7/PARK15 ubiquitin ligase associated with Parkinson's disease. *Biochem J*. 473:3563-3580.

Usher, J.L., J.J. Lee, A. Sanchez-Martinez, and A.J. Whitworth. 2021. Parkin drives pS65-Ub turnover independently of canonical autophagy in Drosophila. *bioRxiv*:2021.2006.2010.447841.

Vincow, E.S., G. Merrihew, R.E. Thomas, N.J. Shulman, R.P. Beyer, M.J. MacCoss, and L.J. Pallanck. 2013. The PINK1-Parkin pathway promotes both mitophagy and selective respiratory chain turnover in vivo. *Proc Natl Acad Sci U S A*. 110:6400-6405.

Whitworth, A.J., J.R. Lee, V.M. Ho, R. Flick, R. Chowdhury, and G.A. McQuibban. 2008. Rhomboid-7 and HtrA2/Omi act in a common pathway with the Parkinson's disease factors Pink1 and Parkin. *Dis Model Mech*. 1:168-174; discussion 173.

Whitworth, A.J., D.A. Theodore, J.C. Greene, H. Benes, P.D. Wes, and L.J. Pallanck. 2005. Increased glutathione S-transferase activity rescues dopaminergic neuron loss in a Drosophila model of Parkinson's disease. *Proc Natl Acad Sci U S A*. 102:8024-8029.

Yamano, K., R. Kikuchi, W. Kojima, R. Hayashida, F. Koyano, J. Kawawaki, T. Shoda, Y. Demizu, M. Naito, K. Tanaka, and N. Matsuda. 2020. Critical role of mitochondrial ubiquitination and the OPTN-ATG9A axis in mitophagy. *J Cell Biol*. 219.

Yamano, K., and R.J. Youle. 2013. PINK1 is degraded through the N-end rule pathway. *Autophagy*. 9:1758-1769.

Yoshii, S.R., and N. Mizushima. 2017. Monitoring and Measuring Autophagy. *Int J Mol Sci*. 18.

Yun, J., R. Puri, H. Yang, M.A. Lizzio, C. Wu, Z.H. Sheng, and M. Guo. 2014. MUL1 acts in parallel to the PINK1/parkin pathway in regulating mitofusin and compensates for loss of PINK1/parkin. *Elife*. 3:e01958.

Zheng, J., X. Chen, Q. Liu, G. Zhong, and M. Zhuang. 2022. Ubiquitin ligase MARCH5 localizes to peroxisomes to regulate pexophagy. *J Cell Biol*. 221.

Zhou, Z.D., J.C.T. Lee, and E.K. Tan. 2018. Pathophysiological mechanisms linking F-box only protein 7 (FBXO7) and Parkinson's disease (PD). *Mutat Res Rev Mutat Res*. 778:72-78.

Zhou, Z.D., S.P. Xie, S. Sathiyamoorthy, W.T. Saw, T.Y. Sing, S.H. Ng, H.P. Chua, A.M. Tang, F. Shaffra, Z. Li, H. Wang, P.G. Ho, M.K. Lai, D.C. Angeles, T.M. Lim, and E.K. Tan. 2015. F-box protein 7 mutations promote protein aggregation in mitochondria and inhibit mitophagy. *Hum Mol Genet*. 24:6314-6330.

Ziviani, E., R.N. Tao, and A.J. Whitworth. 2010. Drosophila parkin requires PINK1 for mitochondrial translocation and ubiquitinates mitofusin. *Proc Natl Acad Sci U S A*. 107:5018-5023.

Figure 1

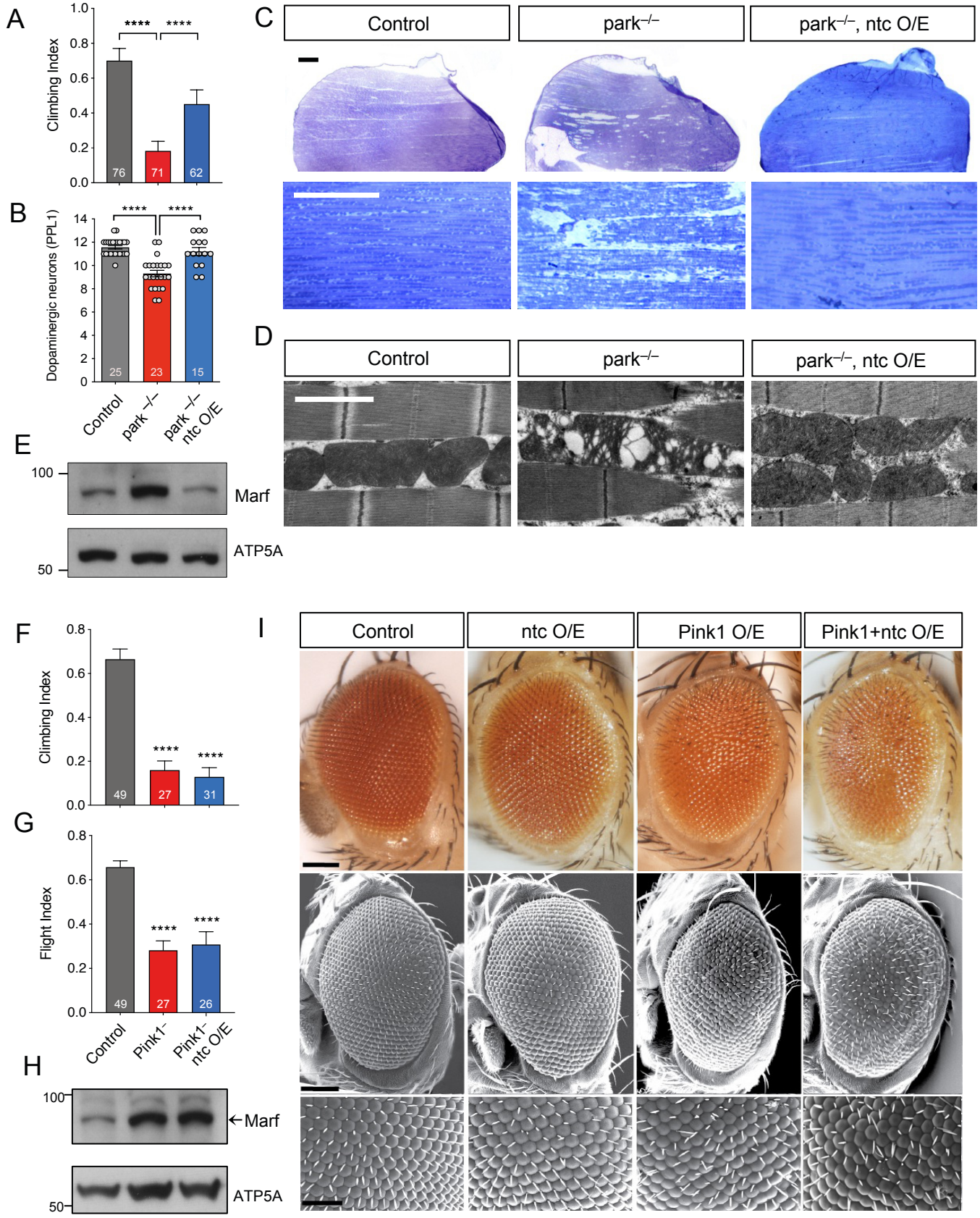
A
Climbing Index
1.0
0.8
0.6
0.4
0.2
0.0
****
****
76
71
62
B
Dopaminergic neurons (PPL1)
14
12
10
8
6
4
2
0
****
****
25
23
15
Control
park −/−
park −/− ntc O/E
C
Control
park−/−
park−/−, ntc O/E
D
Control
park−/−
park−/−, ntc O/E
E
100
Marf
ATP5A
50
F
Climbing Index
0.8
0.6
0.4
0.2
0.0
****
****
49
27
31
G
Flight Index
0.8
0.6
0.4
0.2
0.0
****
****
49
27
26
Control
Pink1−
Pink1− ntc O/E
H
100
Marf
ATP5A
50
I
Control
ntc O/E
Pink1 O/E
Pink1+ntc O/E

Figure 2

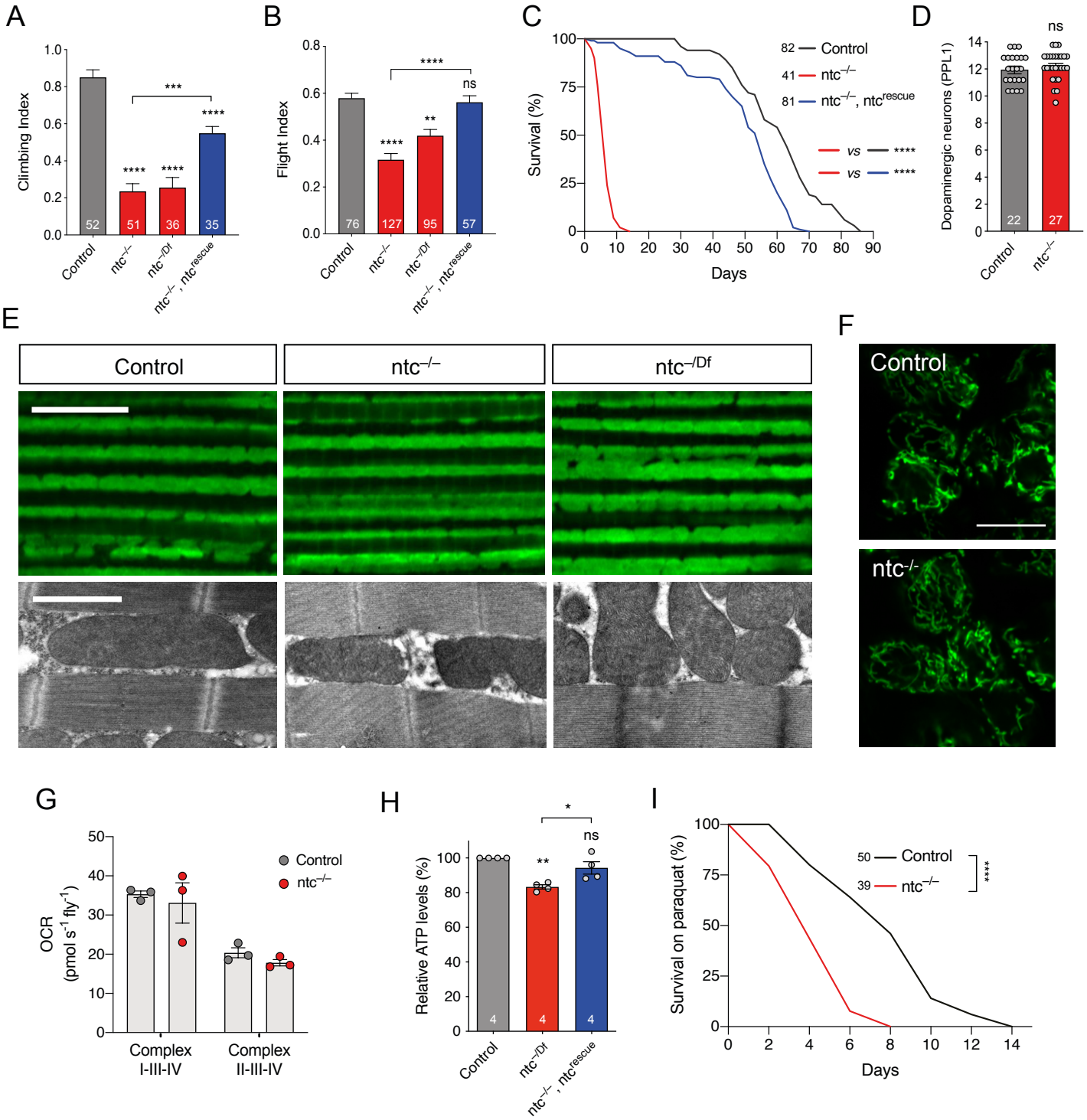
A
Climbing Index
1.0
0.8
0.6
0.4
0.2
0.0
***
****
****
****
52
51
36
35
Control
ntc−/−
ntc−/Df
ntc−/−, ntcrescue
B
Flight Index
0.8
0.6
0.4
0.2
0.0
****
****
**
ns
76
127
95
57
Control
ntc−/−
ntc−/Df
ntc−/−, ntcrescue
C
Survival (%)
100
75
50
25
0
0
10
20
30
40
50
60
70
80
90
Days
82 Control
41 ntc−/−
81 ntc−/−, ntcrescue
vs ****
vs ****
D
Dopaminergic neurons (PPL1)
14
12
10
8
6
4
2
0
ns
22
27
Control
ntc−/−
E
Control
ntc−/−
ntc−/Df
F
Control
ntc-/-
G
OCR
(pmol s-1 fly-1)
50
40
30
20
10
0
Control
ntc−/−
Complex
I-III-IV
Complex
II-III-IV
H
Relative ATP levels (%)
100
80
60
40
20
0
*
**
ns
4
4
4
Control
ntc−/Df
ntc−/−, ntcrescue
I
Survival on paraquat (%)
100
75
50
25
0
0
2
4
6
8
10
12
14
Days
50 Control
39 ntc−/−
****

Figure 3

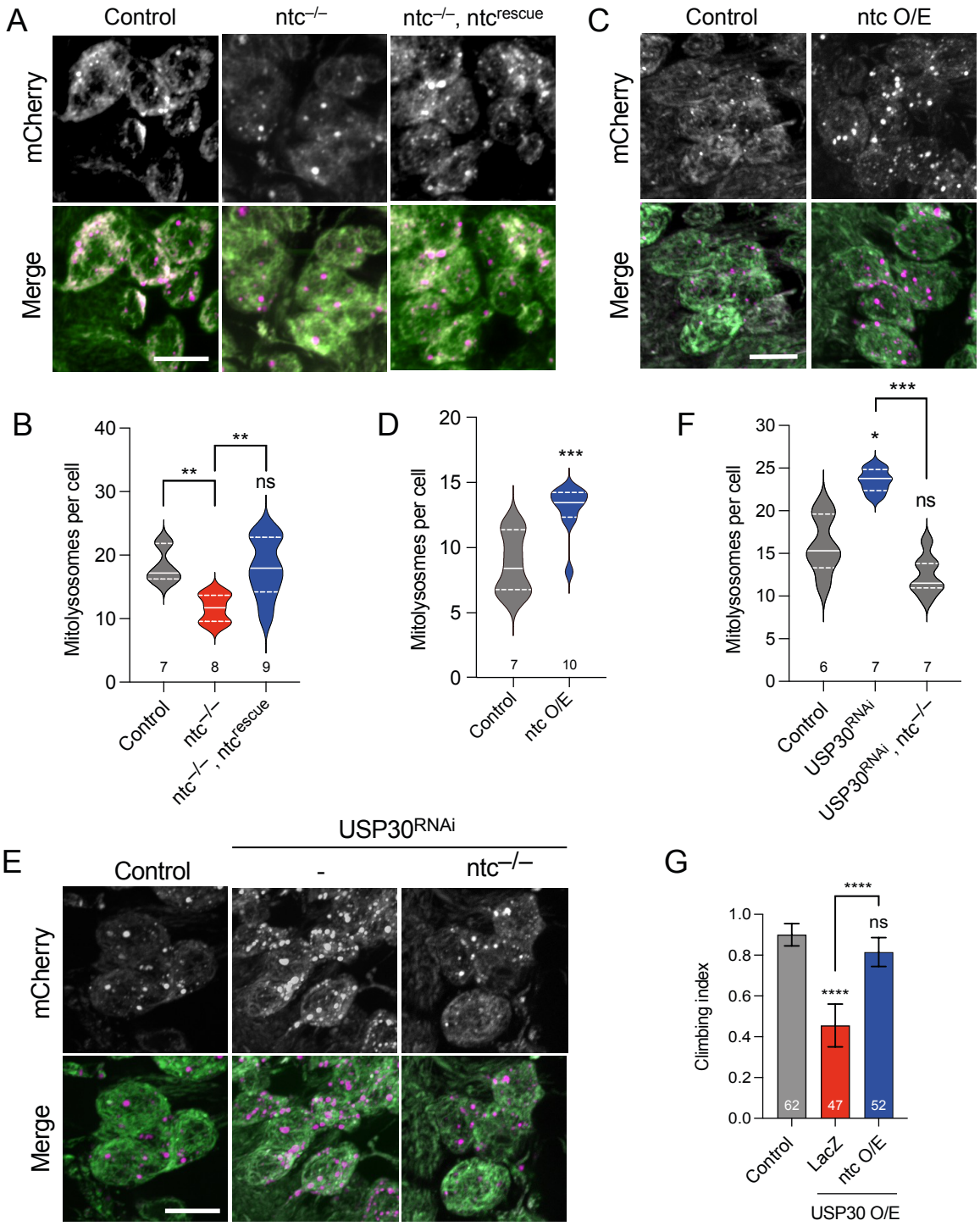
A
Control
ntc−/−
ntc−/−, ntcrescue
mCherry
Merge
C
Control
ntc O/E
mCherry
Merge
B
Mitolysosomes per cell
40
30
20
10
0
**
**
ns
7
8
9
Control
ntc−/−
ntc−/−, ntcrescue
D
Mitolysosmes per cell
20
15
10
5
0
***
7
10
Control
ntc O/E
F
Mitolysosomes per cell
30
25
20
15
10
5
0
*
***
ns
6
7
7
Control
USP30RNAi
USP30RNAi, ntc−/−
E
USP30RNAi
Control
-
ntc−/−
mCherry
Merge
G
Climbing index
1.0
0.8
0.6
0.4
0.2
0.0
****
****
ns
62
47
52
Control
LacZ
ntc O/E
USP30 O/E

Figure 4

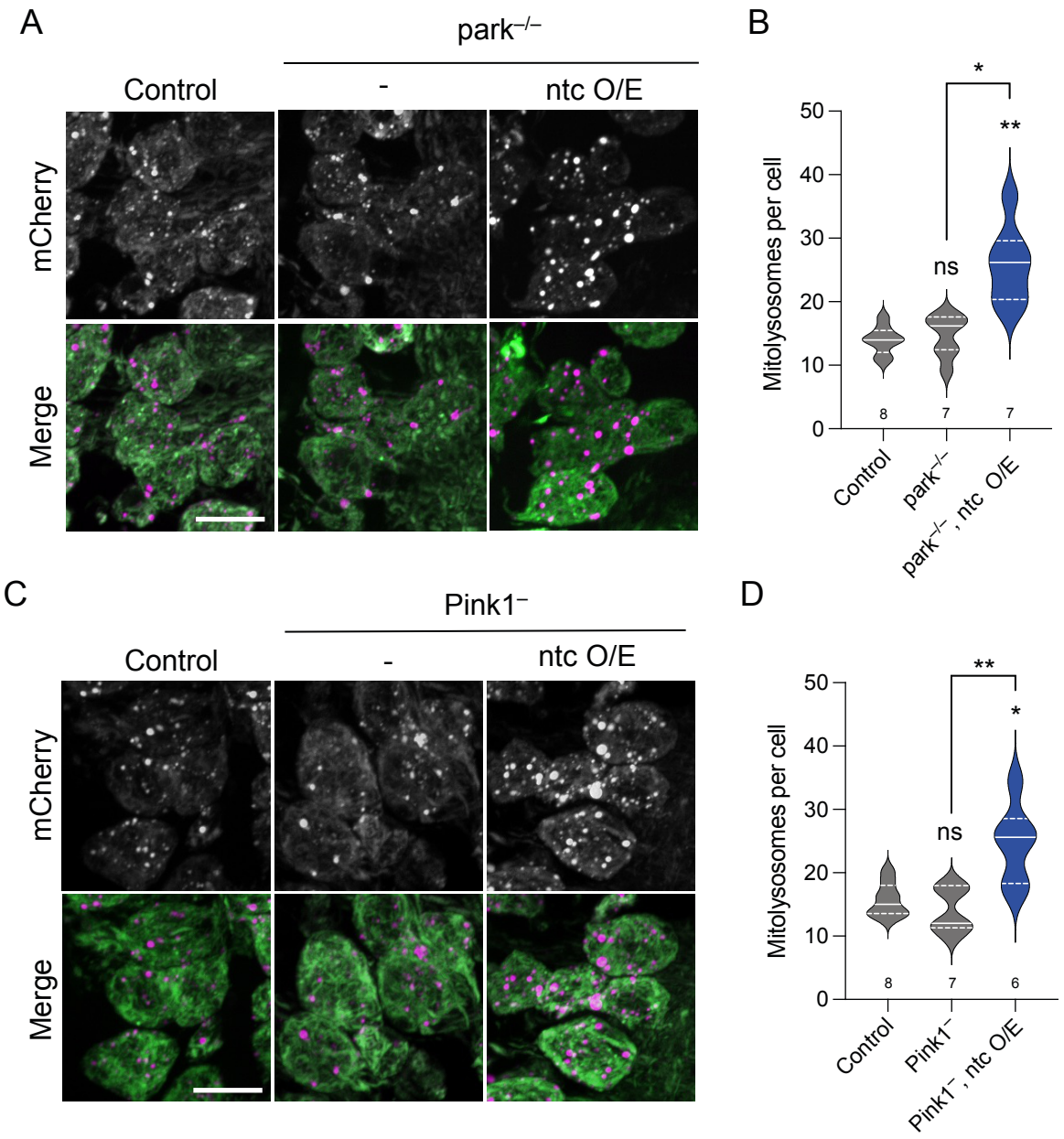
A
park−/−
Control
-
ntc O/E
mCherry
Merge
B
Mitolysosomes per cell
50
40
30
20
10
0
*
**
ns
8
7
7
Control
park−/−
park−/− , ntc O/E
C
Pink1−
Control
-
ntc O/E
mCherry
Merge
D
Mitolysosomes per cell
50
40
30
20
10
0
**
*
ns
8
7
6
Control
Pink1−
Pink1− , ntc O/E

Figure 5

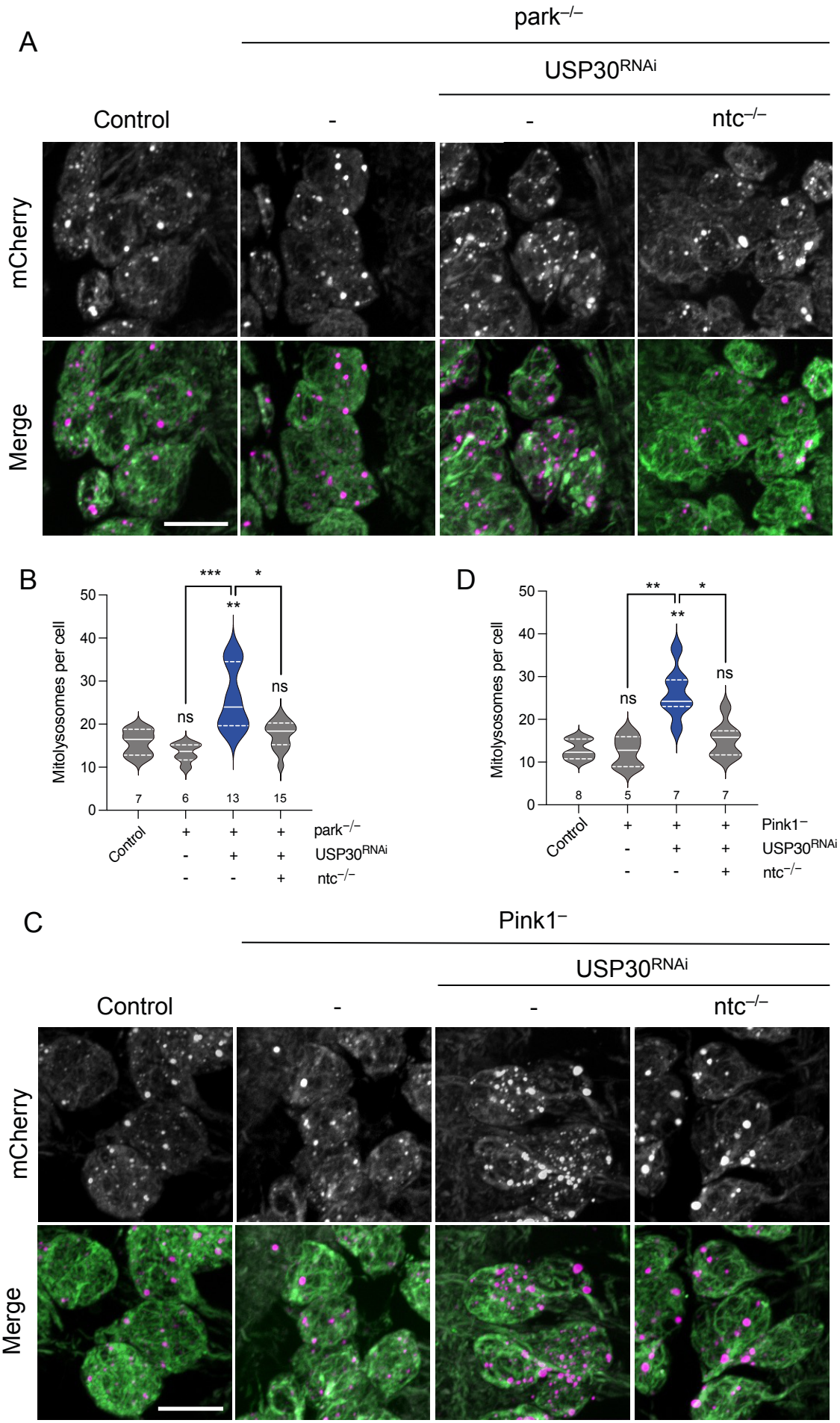
A
park−/−
USP30RNAi
Control
-
-
ntc−/−
mCherry
Merge
B
Mitolysosomes per cell
50
40
30
20
10
0
***
*
**
ns
ns
7
6
13
15
Control
park−/−
USP30RNAi
ntc−/−
D
Mitolysosomes per cell
**
*
**
ns
ns
8
5
7
7
Control
Pink1−
USP30RNAi
ntc−/−
C
Pink1−
USP30RNAi
Control
-
-
ntc−/−
mCherry
Merge

Figure 6

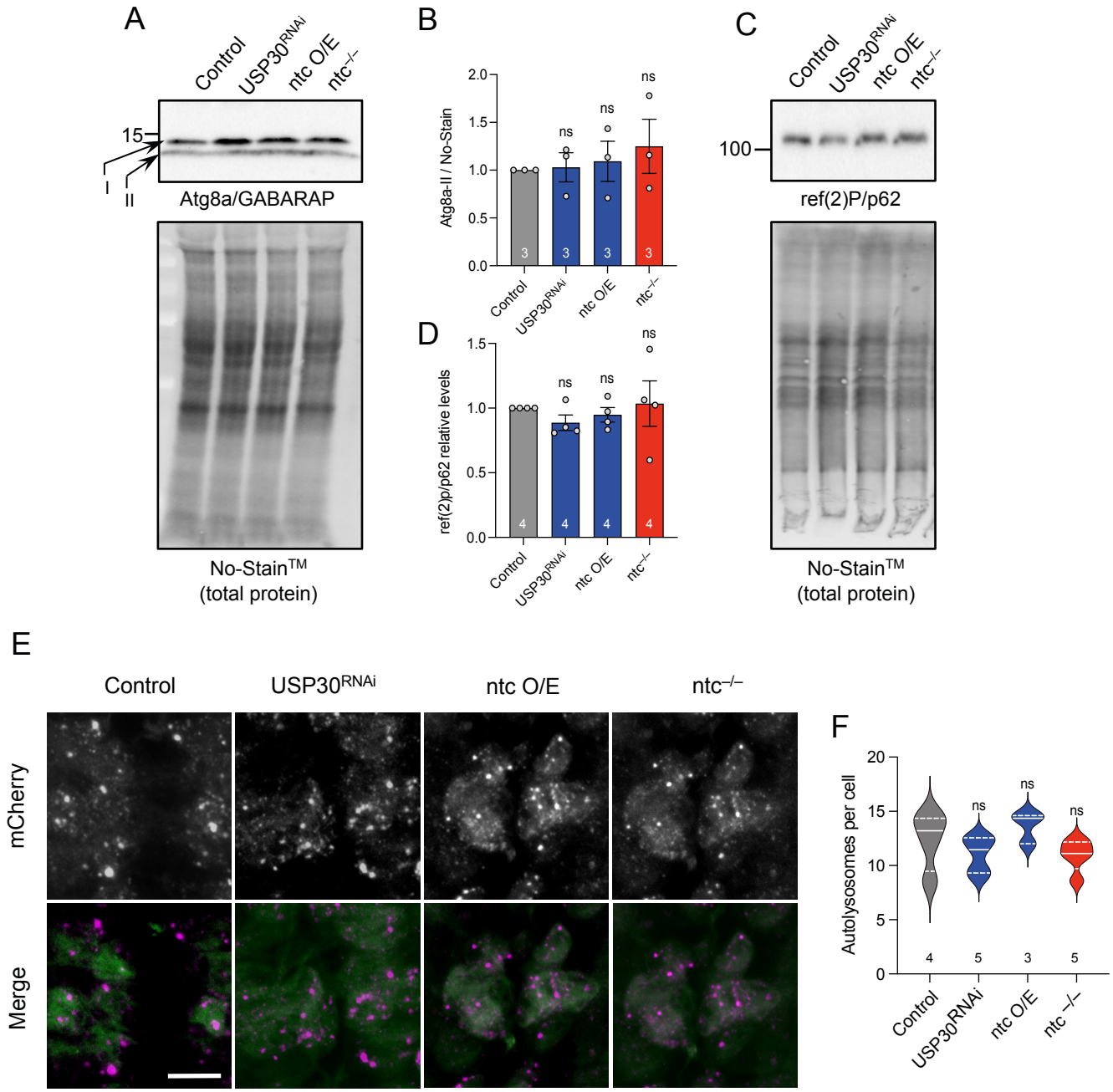
A
Control
USP30RNAi
ntc O/E
ntc−/−
15
I
II
Atg8a/GABARAP
No-Stain™
(total protein)
B
Atg8a-II / No-Stain
2.0
1.5
1.0
0.5
0.0
ns
3
Control
USP30RNAi
ntc O/E
ntc−/−
C
100
ref(2)P/p62
No-Stain™
(total protein)
D
ref(2)p/p62 relative levels
4
E
Control
USP30RNAi
ntc O/E
ntc−/−
mCherry
Merge
F
Autolysosomes per cell
20
15
10
5
0
4
5
3
5

Figure 7

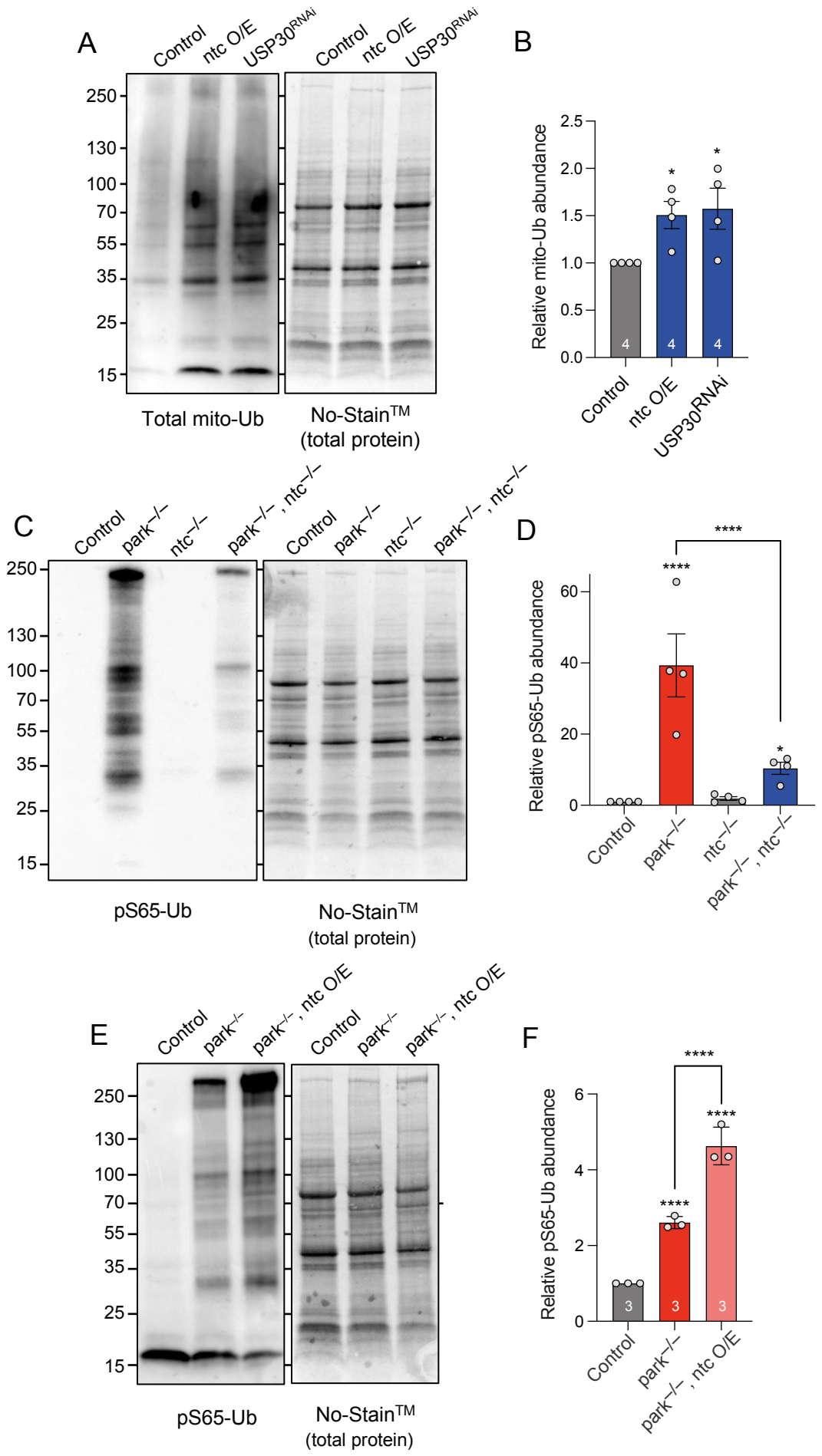
A
Control
ntc O/E
USP30RNAi
Control
ntc O/E
USP30RNAi
250
130
100
70
55
35
25
15
Total mito-Ub
No-Stain™
(total protein)
B
Relative mito-Ub abundance
2.5
2.0
1.5
1.0
0.5
0.0
4
4
4
Control
ntc O/E
USP30RNAi
C
Control
park−/−
ntc−/−
park−/−, ntc−/−
Control
park−/−
ntc−/−
park−/−, ntc−/−
250
130
100
70
55
35
25
15
pS65-Ub
No-Stain™
(total protein)
D
Relative pS65-Ub abundance
60
40
20
0
****
****
*
Control
park−/−
ntc−/−
park−/−, ntc−/−
E
Control
park−/−
park−/−, ntc O/E
Control
park−/−
park−/−, ntc O/E
250
130
100
70
55
35
25
15
pS65-Ub
No-Stain™
(total protein)
F
Relative pS65-Ub abundance
6
4
2
0
****
****
****
3
3
3
Control
park−/−
park−/−, ntc O/E

Figure 8

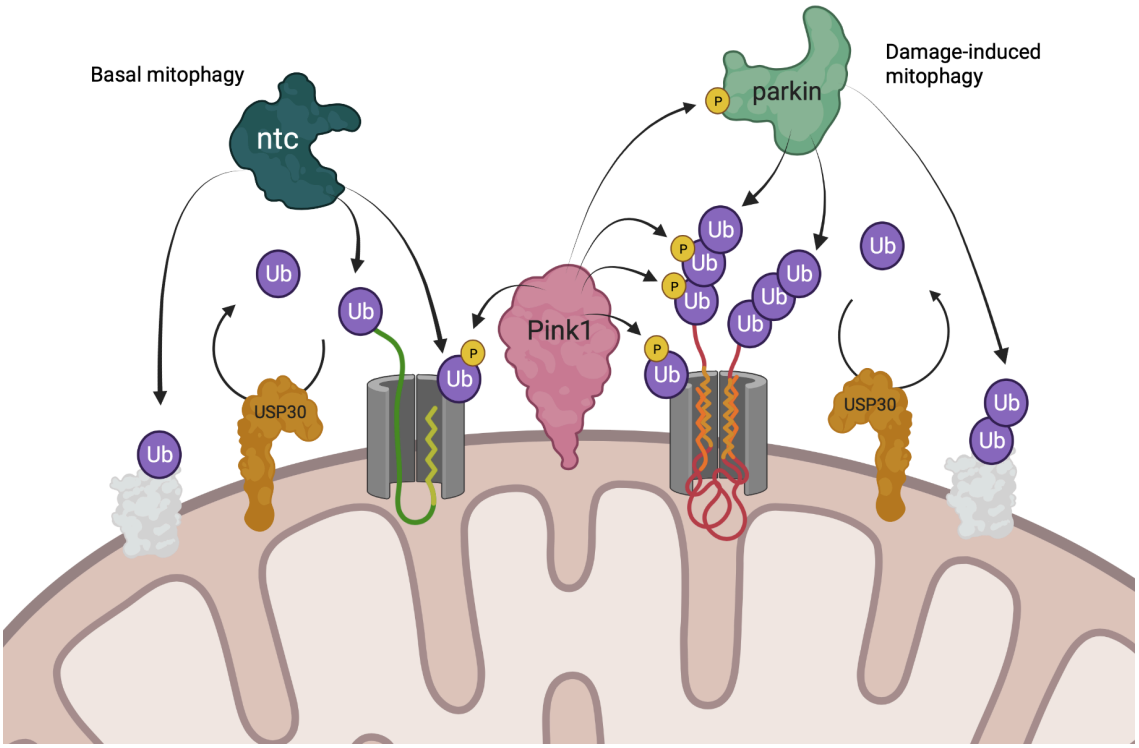

Basal mitophagy
ntc
parkin
Damage-induced mitophagy
Pink1
Ub
P
USP30

Figure S1

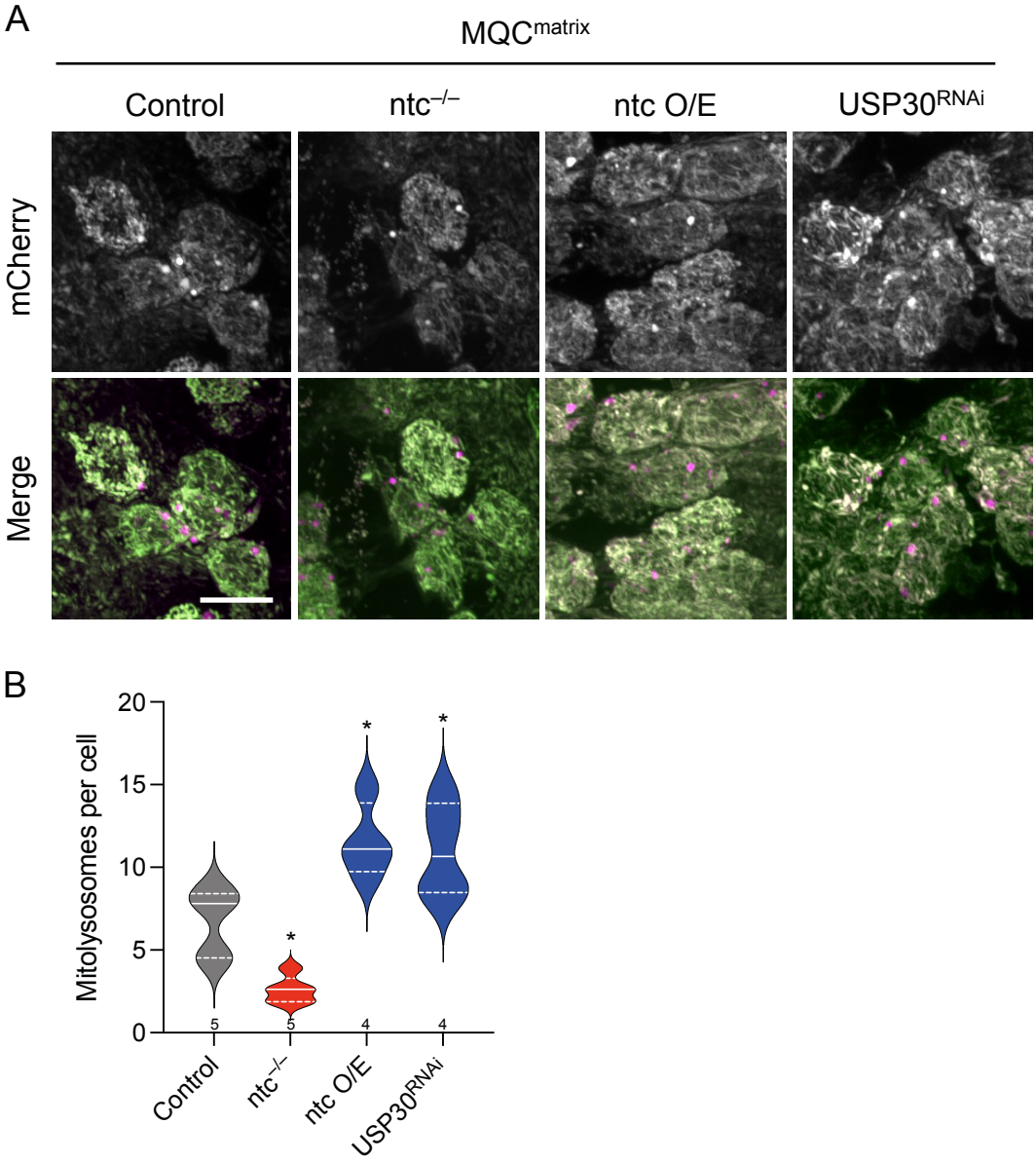
A
MQC^matrix
Control
ntc−/−
ntc O/E
USP30^RNAi
mCherry
Merge
B
Mitolysosomes per cell
20
15
10
5
0
*
*
*
5
5
4
4
Control
ntc−/−
ntc O/E
USP30^RNAi

Figure S2

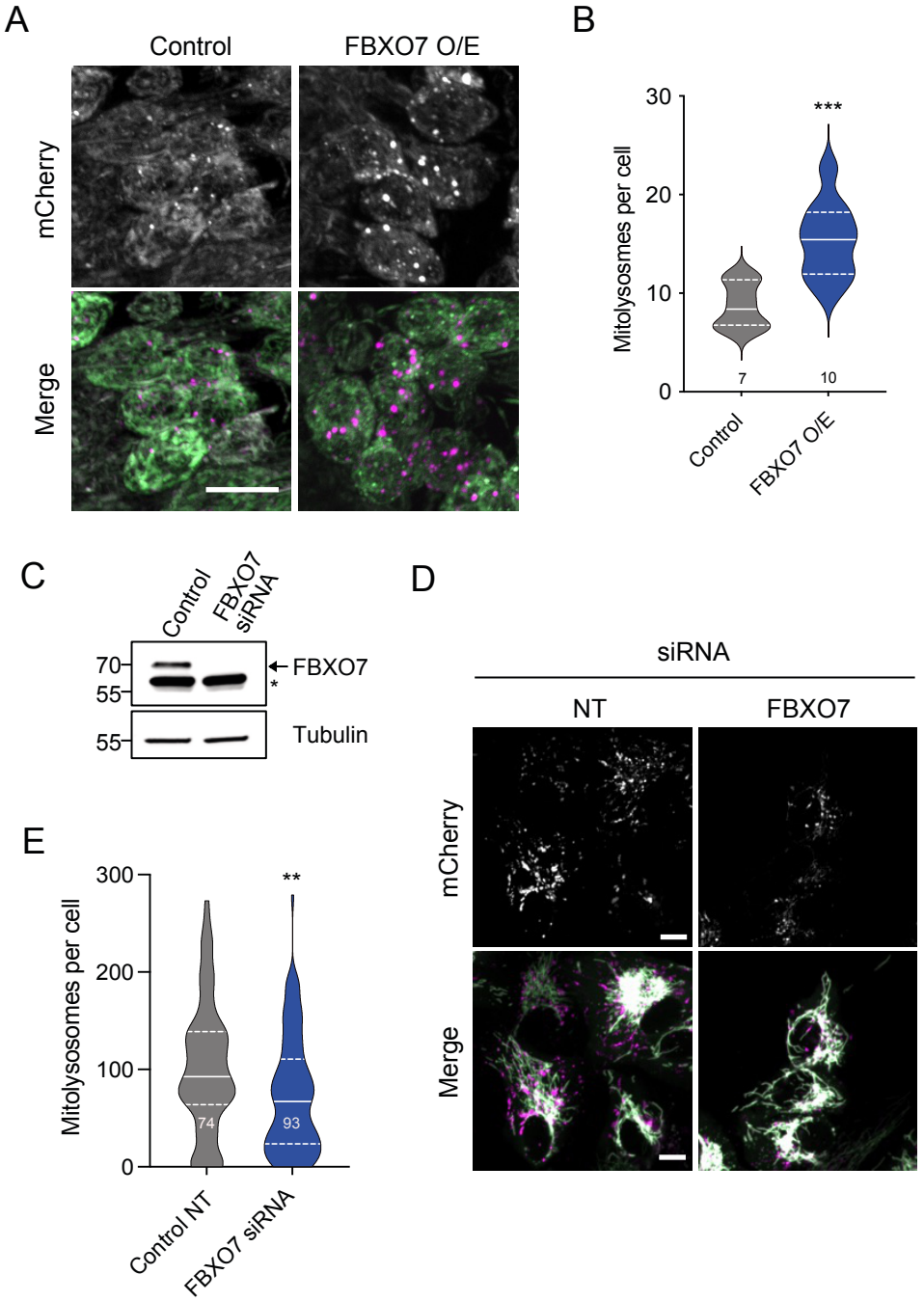
A
Control
FBXO7 O/E
mCherry
Merge
B
Mitolysosmes per cell
30
20
10
0
***
7
10
Control
FBXO7 O/E
C
Control
FBXO7 siRNA
70
55
FBXO7
*
55
Tubulin
D
siRNA
NT
FBXO7
mCherry
Merge
E
Mitolysosomes per cell
300
200
100
0
**
74
93
Control NT
FBXO7 siRNA

Figure S3

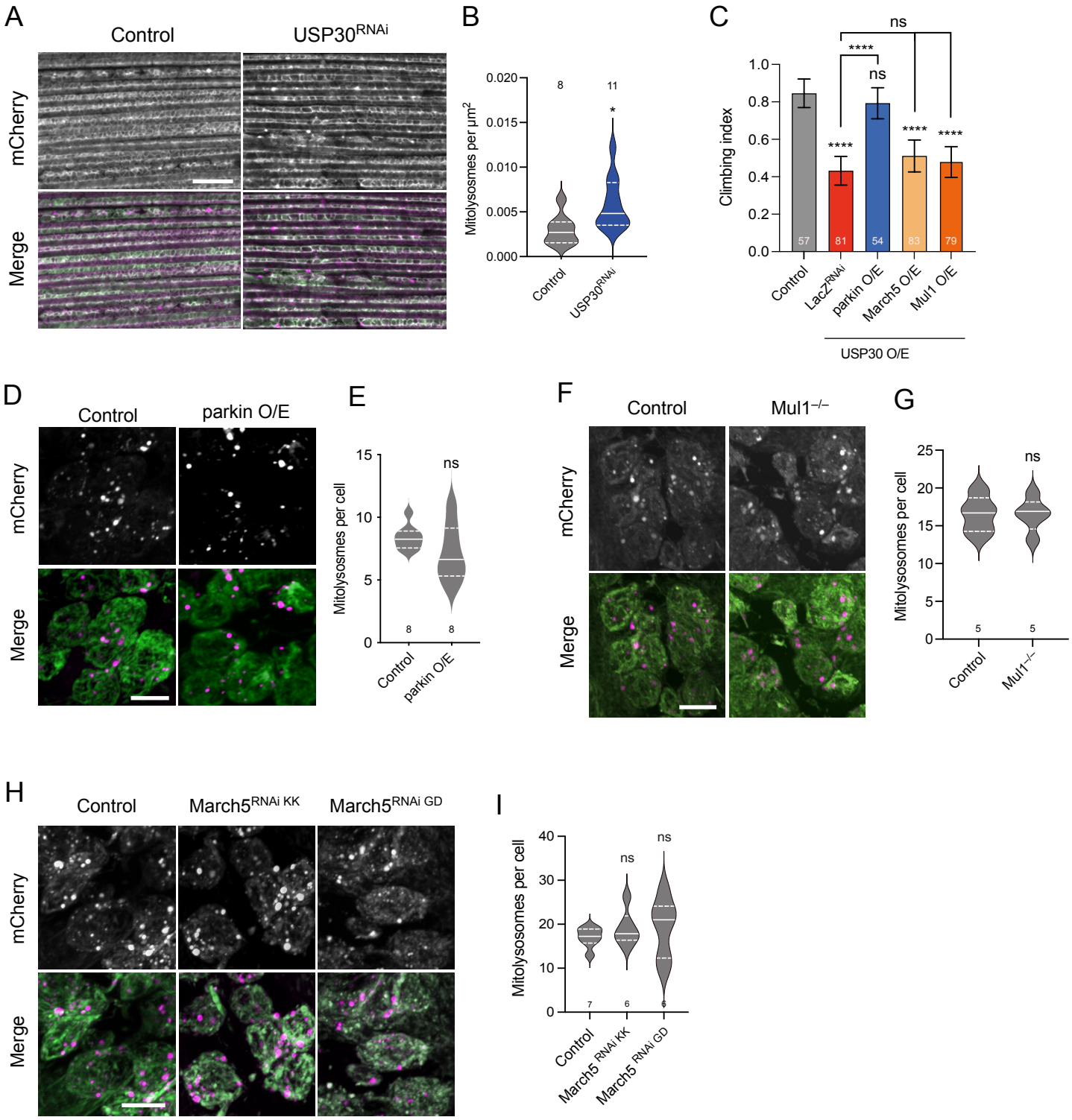
A
Control
USP30RNAi
mCherry
Merge
B
Mitolysosmes per μm2
0.020
0.015
0.010
0.005
0.000
8
11
*
Control
USP30RNAi
C
Climbing index
1.0
0.8
0.6
0.4
0.2
0.0
ns
****
ns
****
****
****
57
81
54
83
79
Control
LacZRNAi
parkin O/E
March5 O/E
Mul1 O/E
USP30 O/E
D
Control
parkin O/E
mCherry
Merge
E
Mitolysosmes per cell
15
10
5
0
ns
8
8
Control
parkin O/E
F
Control
Mul1−/−
mCherry
Merge
G
Mitolysosomes per cell
25
20
15
10
5
0
ns
5
5
Control
Mul1−/−
H
Control
March5RNAi KK
March5RNAi GD
mCherry
Merge
I
Mitolysosomes per cell
40
30
20
10
0
ns
ns
7
6
6
Control
March5 RNAi KK
March5 RNAi GD

Figure S4

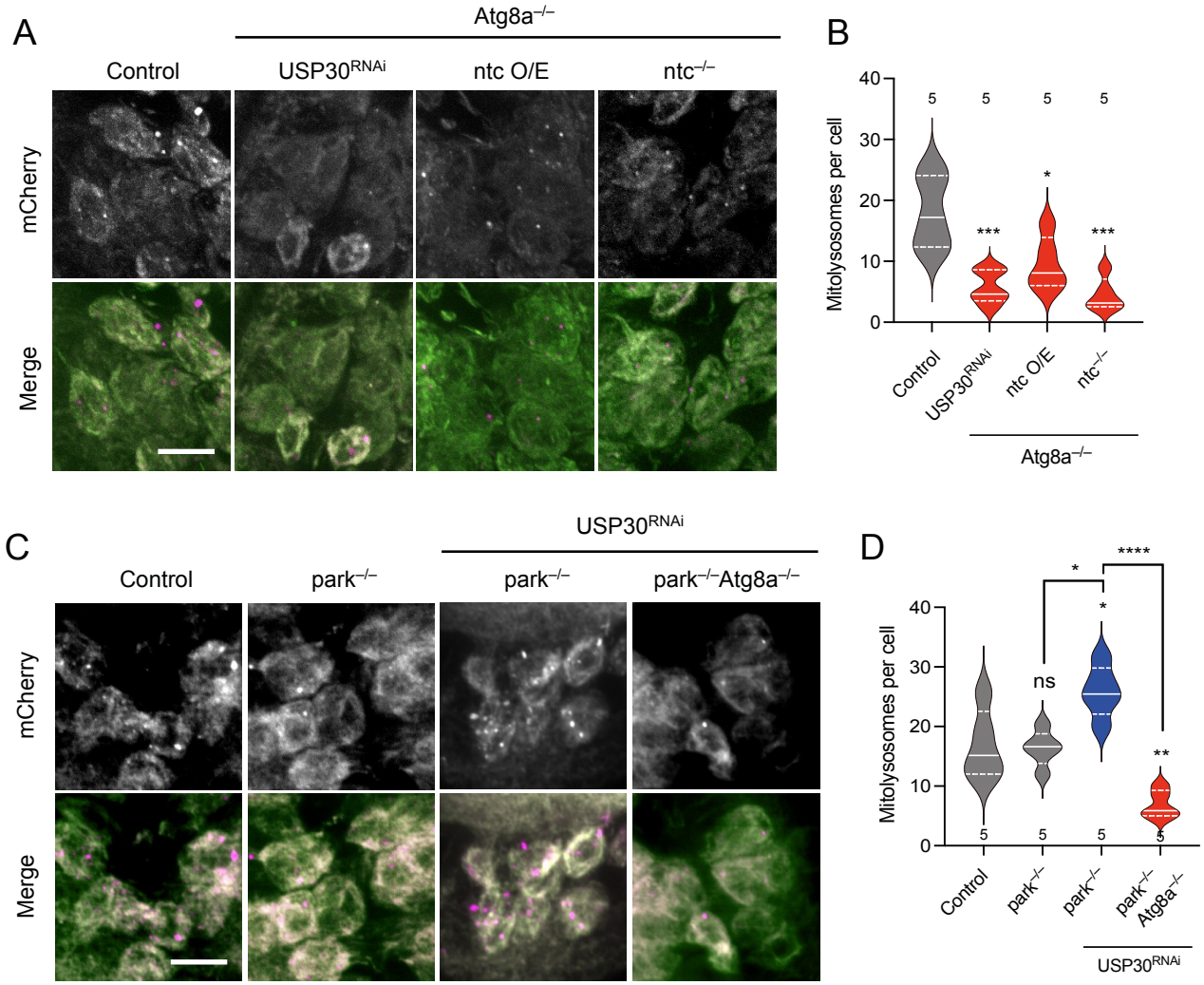
A
Atg8a−/−
Control
USP30RNAi
ntc O/E
ntc−/−
mCherry
Merge
B
Mitolysosomes per cell
40
30
20
10
0
5
5
5
5
***
*
***
Control
USP30RNAi
ntc O/E
ntc−/−
Atg8a−/−
C
USP30RNAi
Control
park−/−
park−/−
park−/−Atg8a−/−
mCherry
Merge
D
Mitolysosomes per cell
40
30
20
10
0
*
****
ns
*
**
5
5
5
5
Control
park−/−
park−/−
park−/−
Atg8a−/−
USP30RNAi

Supplementary Table 1. Details of full genotypes used in this study. More details of each line can be found in Methods.

Figure 1	
Label	**Genotype**
A	
Control	UAS-LacZ/+; da-GAL4/+
park$^{-/-}$	UAS-LacZ/+; da-GAL4, park^{25}/park^{25}
park$^{-/-}$; ntc O/E	UAS-ntc/+; da-GAL4, park^{25}/park^{25}
B	
Control	UAS-LacZ/+; da-GAL4/+
park$^{-/-}$	UAS-LacZ/+; da-GAL4, park^{25}/park^{25}
park$^{-/-}$; ntc O/E	UAS-ntc/+; da-GAL4, park^{25}/park^{25}
C	
Control	UAS-LacZ/+; da-GAL4/+
park$^{-/-}$	UAS-LacZ/+; da-GAL4, park^{25}/park^{25}
park$^{-/-}$; ntc	UAS-ntc/+; da-GAL4, park^{25}/park^{25}
D	
Control	UAS-LacZ/+; da-GAL4/+
park$^{-/-}$	UAS-LacZ/+; da-GAL4, park^{25}/park^{25}
park$^{-/-}$; ntc O/E	UAS-ntc/+; da-GAL4, park^{25}/park^{25}
E	
Control	UAS-LacZ/+; da-GAL4/+
park$^{-/-}$	UAS-LacZ/+; da-GAL4, park^{25}/park^{25}
park$^{-/-}$; ntc O/E	UAS-ntc/+; da-GAL4, park^{25}/park^{25}
F	
Control	UAS-LacZ/+; da-GAL4/+
Pink1^{-}	Pink1^{B9}/Y; UAS-LacZ/+; da-GAL4/+

Pink1^{-}; ntc O/E	Pink1^{B9}/Y; UAS-ntc/+; da-GAL4/+
G	
Control	UAS-LacZ/+; da-GAL4/+
Pink1^{-}	Pink1^{B9}/Y; UAS-LacZ/+; da-GAL4/+
Pink1^{-}; ntc O/E	Pink1^{B9}/Y; UAS-ntc/+; da-GAL4/+
H	
Control	UAS-LacZ/+; da-GAL4/+
Pink1^{-}	Pink1^{B9}/Y; UAS-LacZ/+; da-GAL4/+
Pink1^{-}; ntc O/E	Pink1^{B9}/Y; UAS-ntc/+; da-GAL4/+
I	
Control	GMR-GAL4/UAS-LacZ
ntc O/E	GMR-GAL4, UAS-LacZ/UAS-ntc
Pink1 O/E	GMR-GAL4, UAS-Pink1/UAS-LacZ
Pink1+ntc O/E	GMR-GAL4, UAS-Pink1/UAS-ntc

Figure 2	
Label	**Genotype**
A	
Control	UAS-LacZ/+; da-GAL4/+
ntc$^{-/-}$	ntc^{ms771}/ntc^{ms771}
ntc$^{-/Df}$	ntc^{ms771}/Df(3L)Exel6097
ntc$^{-/-}$, ntc^{rescue}	UAS-ntc; da-GAL4, ntc^{ms771}/ ntc^{ms771}
B	
Control	UAS-LacZ/+; da-GAL4/+
ntc$^{-/-}$	ntc^{ms771}/ntc^{ms771}
ntc$^{-/Df}$	ntc^{ms771}/Df(3L)Exel6097

ntc$^{-/-}$, ntc^{rescue}	UAS-ntc; da-GAL4, ntc^{ms771}/ ntc^{ms771}
C	
Control	w^{1118}
ntc$^{-/-}$	ntc^{ms771}/ntc^{ms771}
ntc$^{-/-}$, ntc^{rescue}	UAS-ntc; da-GAL4, ntc^{ms771}/ntc^{ms771}
D	
Control	w^{1118}
ntc$^{-/-}$	ntc^{ms771}/ntc^{ms771}
E	
Control	UAS-LacZ/+; da-GAL4/+
ntc$^{-/-}$	ntc^{ms771}/ntc^{ms771}
ntc$^{-/Df}$	ntc^{ms771}/Df(3L)Exel6097
F	
Control	w^{1118}
ntc$^{-/-}$	ntc^{ms771}/ntc^{ms771}
G	
Control	w^{1118}
ntc$^{-/-}$	ntc^{ms771}/ntc^{ms771}
H	
Control	w^{1118}
ntc$^{-/-}$	ntc^{ms771}/ntc^{ms771}
ntc$^{-/-}$, ntc^{rescue}	UAS-ntc; da-GAL4, ntc^{ms771}/ntc^{ms771}
I	
Control	w^{1118}
ntc$^{-/-}$	ntc^{ms771}/ntc^{ms771}

Figure 3	
Label	**Genotype**
A	
Control	mito-QC/UAS-LacZ^{RNAi}; nSyb-GAL4/+
ntc$^{-/-}$	mito-QC/UAS-LacZ^{RNAi}; nSyb-GAL4, ntc^{ms771}/ntc^{ms771}
ntc$^{-/-}$, ntc^{rescue}	mito-QC/UAS-ntc; nSyb-GAL4, ntc^{ms771}/ntc^{ms771}
B	
Control	mito-QC/UAS-LacZ^{RNAi}; nSyb-GAL4/+
ntc$^{-/-}$	mito-QC/UAS-LacZ^{RNAi}; nSyb-GAL4, ntc^{ms771}/ntc^{ms771}
ntc$^{-/-}$, ntc^{rescue}	mito-QC/UAS-ntc; nSyb-GAL4, ntc^{ms771}/ntc^{ms771}
C	
Control	mito-QC/UAS-LacZ^{RNAi}; nSyb-GAL4/+
ntc O/E	mito-QC/UAS-ntc; nSyb-GAL4/+
D	
Control	mito-QC/UAS-LacZ^{RNAi}; nSyb-GAL4/+
ntc O/E	mito-QC/UAS-ntc; nSyb-GAL4/+
E	
Control	mito-QC/UAS-LacZ^{RNAi}; nSyb-GAL4/+
USP30^{RNAi}	mito-QC/UAS-USP30^{RNAi}; nSyb-GAL4/+
USP30^{RNAi}, ntc$^{-/-}$	mito-QC/UAS-USP30^{RNAi}; nSyb-GAL4, ntc^{ms771}/ntc^{ms771}
F	
Control	mito-QC/UAS-LacZ^{RNAi}; nSyb-GAL4/+
USP30^{RNAi}	mito-QC/UAS-USP30^{RNAi}; nSyb-GAL4/+
USP30^{RNAi}, ntc$^{-/-}$	mito-QC/UAS-USP30^{RNAi}; nSyb-GAL4, ntc^{ms771}/ntc^{ms771}
G	
Control	Act-GAL4/UAS-LacZ

USP30 O/E + LacZ	Act-GAL4, UAS-USP30/UAS-LacZ
USP30 O/E + ntc O/E	Act-GAL4, UAS-USP30/UAS-ntc

Figure 4	
Label	**Genotype**
A	
Control	mito-QC/UAS-LacZ^{RNAi}; nSyb-GAL4/+
park$^{-/-}$	mito-QC/UAS-LacZ^{RNAi}; nSyb-GAL4, park^{25}/park^{25}
park$^{-/-}$, ntc O/E	mito-QC/UAS-ntc; nSyb-GAL4, park^{25}/park^{25}
B	
Control	mito-QC/UAS-LacZ^{RNAi}; nSyb-GAL4/+
park$^{-/-}$	mito-QC/UAS-LacZ^{RNAi}; nSyb-GAL4, park^{25}/park^{25}
park$^{-/-}$, ntc O/E	mito-QC/UAS-ntc; nSyb-GAL4, park^{25}/park^{25}
C	
Control	mito-QC/UAS-LacZ^{RNAi}; nSyb-GAL4/+
Pink1^{-}	Pink1^{B9}/Y; mito-QC/UAS-LacZ^{RNAi}; nSyb-GAL4/+
Pink1^{-}, ntc O/E	Pink1^{B9}/Y; mito-QC/UAS-ntc; nSyb-GAL4/+
D	
Control	mito-QC/UAS-LacZ^{RNAi}; nSyb-GAL4/+
Pink1^{-}	Pink1^{B9}/Y; mito-QC/UAS-LacZ^{RNAi}; nSyb-GAL4/+
Pink1^{-}, ntc O/E	Pink1^{B9}/Y; mito-QC/UAS-ntc; nSyb-GAL4/+

Figure 5	
Label	**Genotype**
A	
Control	mito-QC/UAS-LacZ^{RNAi}; nSyb-GAL4/+

park$^{-/-}$	mito-QC/UAS-LacZ^{RNAi}; nSyb-GAL4, park^{25}/park^{25}
park$^{-/-}$, USP30^{RNAi}	mito-QC/UAS-USP30^{RNAi}; nSyb-GAL4, park^{25}/park^{25}
park$^{-/-}$, USP30^{RNAi}, ntc$^{-/-}$	mito-QC/UAS-USP30^{RNAi}; nSyb-GAL4, park^{25}, PBac{WH}CG10855^{f07259}/ntc^{ms771}
B	
Control	mito-QC/UAS-LacZ^{RNAi}; nSyb-GAL4/+
park$^{-/-}$	mito-QC/UAS-LacZ^{RNAi}; nSyb-GAL4, park^{25}/park^{25}
park$^{-/-}$, USP30^{RNAi}	mito-QC/UAS-USP30^{RNAi}; nSyb-GAL4, park^{25}/park^{25}
park$^{-/-}$, USP30^{RNAi}, ntc$^{-/-}$	mito-QC/UAS-USP30^{RNAi}; nSyb-GAL4, park^{25}, PBac{WH}CG10855^{f07259}/ntc^{ms771}
C	
Control	mito-QC/ UAS-LacZ^{RNAi}; nSyb-GAL4/+
Pink1^{-}	Pink1^{B9}/Y; mito-QC/UAS-LacZ^{RNAi}; nSyb-GAL4/+
Pink1^{-}, USP30^{RNAi}	Pink1^{B9}/Y; mito-QC/UAS-USP30^{RNAi}; nSyb-GAL4/+
Pink1^{-}, USP30^{RNAi}, ntc$^{-/-}$	Pink1^{B9}/Y; mito-QC/UAS-USP30^{RNAi}; nSyb-GAL4, ntc^{ms771}/ntc^{ms771}
D	
Control	mito-QC/ UAS-LacZ^{RNAi}; nSyb-GAL4/+
Pink1^{-}	Pink1^{B9}/Y; mito-QC/UAS-LacZ^{RNAi}; nSyb-GAL4/+
Pink1^{-}, USP30^{RNAi}	Pink1^{B9}/Y; mito-QC/UAS-USP30^{RNAi}; nSyb-GAL4/+
Pink1^{-}, USP30^{RNAi}, ntc$^{-/-}$	Pink1^{B9}/Y; mito-QC/UAS-USP30^{RNAi}; nSyb-GAL4, ntc^{ms771}/ntc^{ms771}

Figure 6	
Label	**Genotype**
A	
Control	UAS-LacZ/+; da-GAL4/+
USP30^{RNAi}	UAS-USP30^{RNAi}/+; da-GAL4/+

ntc O/E	UAS-ntc/+; da-GAL4/+
ntc$^{-/-}$	ntc^{ms771}/ntc^{ms771}
B	
Control	UAS-LacZ/+; da-GAL4/+
USP30^{RNAi}	UAS-USP30^{RNAi}/+; da-GAL4/+
ntc O/E	UAS-ntc/+; da-GAL4/+
ntc$^{-/-}$	ntc^{ms771}/ntc^{ms771}
C	
Control	UAS-LacZ/+; da-GAL4/+
USP30^{RNAi}	UAS-USP30^{RNAi}/+; da-GAL4/+
ntc O/E	UAS-ntc/+; da-GAL4/+
ntc$^{-/-}$	ntc^{ms771}/ntc^{ms771}
D	
Control	UAS-LacZ/+; da-GAL4/+
USP30^{RNAi}	UAS-USP30^{RNAi}/+; da-GAL4/+
ntc O/E	UAS-ntc/+; da-GAL4/+
ntc$^{-/-}$	ntc^{ms771}/ntc^{ms771}
E	
Control	UAS-GFP-mCherry-Atg8a/UAS-LacZ^{RNAi}/+; nSyb-GAL4/+
USP30^{RNAi}	UAS-GFP-mCherry-Atg8a/UAS-USP30^{RNAi}/+; nSyb-GAL4/+
ntc O/E	UAS-GFP-mCherry-Atg8a/UAS-ntc/+; nSyb-GAL4/+
ntc$^{-/-}$	UAS-GFP-mCherry-Atg8a/UAS-LacZ^{RNAi}/+; nSyb-GAL4, ntc^{ms771}/ntc^{ms771}
F	
Control	UAS-GFP-mCherry-Atg8a/UAS-LacZ^{RNAi}/+; nSyb-GAL4/+
USP30^{RNAi}	UAS-GFP-mCherry-Atg8a/UAS-USP30^{RNAi}/+; nSyb-GAL4/+

ntc O/E	UAS-GFP-mCherry-Atg8a/UAS-ntc/+; nSyb-GAL4/+
ntc$^{-/-}$	UAS-GFP-mCherry-Atg8a/UAS-LacZ^{RNAi}/+; nSyb-GAL4, ntc^{ms771}/ntc^{ms771}

Figure 7	
Label	**Genotype**
A	
Control	UAS-LacZ/+; da-GAL4/+
ntc O/E	UAS-ntc/+; da-GAL4/+
USP30^{RNAi}	UAS-USP30^{RNAi}/+; da-GAL4/+
B	
Control	UAS-LacZ/+; da-GAL4/+
ntc O/E	UAS-ntc/+; da-GAL4/+
USP30^{RNAi}	UAS-USP30^{RNAi}/+; da-GAL4/+
C	
Control	w^{1118}
park$^{-/-}$	park^{25}/park^{25}
ntc$^{-/-}$	ntc^{ms771}/PBac{WH}CG10855^{f07259}
park$^{-/-}$, ntc$^{-/-}$	park^{25}, ntc^{ms771}/park^{25}, PBac{WH}CG10855^{f07259}
D	
Control	w^{1118}
park$^{-/-}$	park^{25}/park^{25}
ntc$^{-/-}$	ntc^{ms771}/PBac{WH}CG10855^{f07259}
park$^{-/-}$, ntc$^{-/-}$	park^{25}, ntc^{ms771}/park^{25}, PBac{WH}CG10855^{f07259}
E	
Control	UAS-LacZ/+; da-GAL4/+
park$^{-/-}$	UAS-LacZ/+; da-GAL4, park^{25}/park^{25}

park$^{-/-}$; ntc O/E	UAS-ntc/+; da-GAL4, park^{25}/park^{25}
F	
Control	UAS-LacZ/+; da-GAL4/+
park$^{-/-}$	UAS-LacZ/+; da-GAL4, park^{25}/park^{25}
park$^{-/-}$; ntc O/E	UAS-ntc/+; da-GAL4, park^{25}/park^{25}

Supplementary Figure 1	
Label	**Genotype**
A	
Control	MQC^{matrix}/UAS-LacZ^{RNAi}; nSyb-GAL4/+
USP30^{RNAi}	MQC^{matrix}/UAS-USP30^{RNAi}; nSyb-GAL4/+
ntc	MQC^{matrix}/UAS-ntc; nSyb-GAL4/+
ntc$^{-/-}$	MQC^{matrix}/UAS-LacZ^{RNAi}; nSyb-GAL4, ntc^{ms771}/ntc^{ms771}
B	
Control	MQC^{matrix}/UAS-LacZ^{RNAi}; nSyb-GAL4/+
USP30^{RNAi}	MQC^{matrix}/UAS-USP30^{RNAi}; nSyb-GAL4/+
ntc	MQC^{matrix}/UAS-ntc; nSyb-GAL4/+
ntc$^{-/-}$	MQC^{matrix}/UAS-LacZ^{RNAi}; nSyb-GAL4, ntc^{ms771}/ntc^{ms771}

Supplementary Figure 2	
Label	**Genotype**
A	
Control	mito-QC/UAS-LacZ^{RNAi}; nSyb-GAL4/+
FBXO7 O/E	mito-QC/UAS-FBXO7; nSyb-GAL4/+
B	
Control	mito-QC/UAS-LacZ^{RNAi}; nSyb-GAL4/+

FBXO7 O/E	mito-QC/UAS-FBXO7; nSyb-GAL4/+

Supplementary Figure 3	
Label	**Genotype**
A	
Control	Mef2-GAL4/UAS-LacZ^{RNAi}; mito-QC/+
USP30^{RNAi}	Mef2-GAL4/UAS-USP30^{RNAi}; mito-QC/+
B	
Control	Mef2-GAL4/UAS-LacZ^{RNAi}; mito-QC/+
USP30^{RNAi}	Mef2-GAL4/UAS-USP30^{RNAi}; mito-QC/+
C	
Control	Act-GAL4/UAS-LacZ
USP30 O/E + LacZ	Act-GAL4, UAS-USP30/UAS-LacZ
USP30 O/E + parkin O/E	Act-GAL4, UAS-USP30/UAS-parkin
USP30 O/E + March5 O/E	Act-GAL4, UAS-USP30/+; UAS-March5/+
USP30 O/E + Mul1 O/E	Act-GAL4, UAS-USP30/+; UAS-Mul1/+
D	
Control	mito-QC/UAS-LacZ^{RNAi}; nSyb-GAL4/+
parkin O/E	mito-QC/UAS- parkin$_{C2}$; nSyb-GAL4/+
E	
Control	mito-QC/UAS-LacZ^{RNAi}; nSyb-GAL4/+
parkin O/E	mito-QC/UAS- parkin$_{C2}$; nSyb-GAL4/+
F	
Control	mito-QC/+; nSyb-GAL4/+
Mul1$^{-/-}$	mito-QC/+; nSyb-GAL4, Mul1[A6]/Mul1[A6]
G	

Control	mito-QC/+; nSyb-GAL4/+
Mul1$^{-/-}$	mito-QC/+; nSyb-GAL4, Mul1[A6]/Mul1[A6]
H	
Control	mito-QC/UAS-LacZ^{RNAi}; nSyb-GAL4/+
March5$^{RNAi\ KK}$	mito-QC/UAS-March5$^{RNAi\ KK}$; nSyb-GAL4/+
March5$^{RNAi\ GD}$	mito-QC/UAS-March5$^{RNAi\ GD}$; nSyb-GAL4/+
I	
Control	mito-QC/UAS-LacZ^{RNAi}; nSyb-GAL4/+
March5$^{RNAi\ KK}$	mito-QC/UAS-March5$^{RNAi\ KK}$; nSyb-GAL4/+
March5$^{RNAi\ GD}$	mito-QC/UAS-March5$^{RNAi\ GD}$; nSyb-GAL4/+

Supplementary Figure 4	
Label	**Genotype**
A	
Control	mito-QC/UAS-LacZ^{RNAi}; nSyb-GAL4/+
Atg8a$^{-/-}$, USP30^{RNAi}	Atg8a[KG07569]/Y; mito-QC/UAS-USP30^{RNAi}; nSyb-GAL4/+
Atg8a$^{-/-}$, ntc O/E	Atg8a[KG07569]/Y; mito-QC/UAS-ntc; nSyb-GAL4/+
Atg8a$^{-/-}$, ntc$^{-/-}$	Atg8a[KG07569]/Y; mito-QC/ LacZ^{RNAi}; nSyb-GAL4, ntc^{ms771}/ntc^{ms771}
B	
Control	mito-QC/UAS-LacZ^{RNAi}; nSyb-GAL4/+
Atg8a$^{-/-}$, USP30^{RNAi}	Atg8a[KG07569]/Y; mito-QC/UAS-USP30^{RNAi}; nSyb-GAL4/+
Atg8a$^{-/-}$, ntc O/E	Atg8a[KG07569]/Y; mito-QC/UAS-ntc; nSyb-GAL4/+
Atg8a$^{-/-}$, ntc$^{-/-}$	Atg8a[KG07569]/Y; mito-QC/ LacZ^{RNAi}; nSyb-GAL4, ntc^{ms771}/ntc^{ms771}
C	

Control	mito-QC/UAS-LacZ^{RNAi}; nSyb-GAL4/+
park$^{-/-}$	mito-QC/UAS-LacZ^{RNAi}; nSyb-GAL4, park^{25}/park^{25}
USP30^{RNAi}, park$^{-/-}$	mito-QC/UAS-USP30^{RNAi}; nSyb-GAL4, park^{25}/park^{25}
Atg8a$^{-/-}$, USP30^{RNAi}, park$^{-/-}$	Atg8a[KG07569]/Y; mito-QC/UAS-USP30^{RNAi}; nSyb-GAL4, park^{25}/park^{25}
D	
Control	mito-QC/UAS-LacZ^{RNAi}; nSyb-GAL4/+
park$^{-/-}$	mito-QC/UAS-LacZ^{RNAi}; nSyb-GAL4, park^{25}/park^{25}
USP30^{RNAi}, park$^{-/-}$	mito-QC/UAS-USP30^{RNAi}; nSyb-GAL4, park^{25}/park^{25}
Atg8a$^{-/-}$, USP30^{RNAi}, park$^{-/-}$	Atg8a[KG07569]/Y; mito-QC/UAS-USP30^{RNAi}; nSyb-GAL4, park^{25}/park^{25}